



universität
wien

MASTERARBEIT

Titel der Masterarbeit

„Compressibility and high-pressure behavior of
spodumene-type $\text{LiScGe}_2\text{O}_6$ “

Verfasser

Gregor Hofer, BSc.

angestrebter akademischer Grad

Master of Science (MSc.)

Wien, 2014

Studienkennzahl lt. Studienblatt:

A >066 815<

Studienrichtung lt. Studienblatt:

Mineralogie und Kristallographie

Betreuer:

Prof. Dr. Ronald Miletich-Pawliczek

Compressibility and high-pressure behavior of
spodumene-type $\text{LiScGe}_2\text{O}_6$

Gregor Hofer

June 2014

Declaration

I, Gregor Hofer, hereby declare that this thesis contains no material, which has been submitted or accepted for an award of any other degree or diploma in any university or institution. To the best of my knowledge and belief this thesis contains no material previously published by any other person except where acknowledgment has been made.

June 2014

Acknowledgment

I want to express my deepest gratitude to Ronald Miletich, who offered me the possibility to do my master thesis in his high-pressure group. Despite his limited time, he always supported me with his wisdom and coffee. He lent me his ear whenever the diamond-anvil cell or the instruments bugged me.

Also, I want to give my special thanks to Katharina Scheidl who taught me how to have fun and exasperation with a diamond-anvil cell. She also was helpful with all my small problems, which I encountered along the way.

Herta Effenberger also needs to be mentioned here, who helped me with the fine tuning of my structure refinements.

My thankfulness goes further to the X-Ray Center of the Technical University of Vienna who allowed me to create all the wonderful plots in this work with their software. And also thanks for the coffee!

Last but no least I must need to mention my fellow students here. I am not capable to express in words how much I am grateful to have met that bunch of people. We have been through so much together, good times and bad times. They were a source of inspiration, fun, comfort and everything in between. I believe that nothing can withstand us!

Contents

Declaration	iv
Acknowledgment	vi
1 Introduction	1
1.1 Motivation of this work	1
1.2 Subject of this study	2
2 Materials and methods	2
2.1 Sample material	2
2.2 The diamond-anvil cell	3
2.2.1 Used diamonds	4
2.3 Raman spectroscopy	6
2.4 Pressure gauge	7
2.5 Equation-of-state	7
2.6 X-ray diffractometry	8
3 Results	11
3.1 High-pressure Raman spectra	11
3.2 Crystallography	13
3.3 Isothermal compression	25
4 Discussion	30
4.1 Raman spectra	30
4.2 Compression behavior	30
5 Appendix	36
References	36
List of figures	40
List of tables	41
Deutsche Zusammenfassung	42
Curriculum vitae	43

Abstract

The synthetic clinopyroxene $\text{LiScGe}_2\text{O}_6$ has been investigated with a variety of in-situ high-pressure Raman spectroscopy and x-ray diffraction methods. Three structure refinements at 0.0001, 4.94 and 9.51 GPa were performed. They all reveal the spacegroup $P2_1/c$ for all pressures; lattice parameters are at 0.0001 GPa $a = 9.9999(8) \text{ \AA}$, $b = 9.1040(2) \text{ \AA}$, $c = 5.4610(2) \text{ \AA}$, $\beta = 109.240(2)^\circ$. Series of x-ray diffraction measurements of the lattice dimensions and Raman spectra over a pressure range of 0.0001 to 4.99(1) GPa was obtained. The x-ray data reveal a continuous, smooth line which does not indicate any structural phase transition within the investigated pressure range. This is in line with the results obtained from structure refinements. The lattice data was fitted using a third order Birch-Murnaghan equation-of-state and yielded $V_0 = 469.61(11) \text{ \AA}^3$, $K_0 = 83(2) \text{ GPa}$ and $K' = 7.5(11)$. The Raman spectra confirm that no phase transition occurred. The obtained data was compared to recent high-pressure studies of clinopyroxenes and shows a continuation of the the high-pressure behavior trends set by these studies.

1 Introduction

1.1 Motivation of this work

Pyroxenes make up a major part of the Earth's mantle and are therefore important minerals for the description of the general properties of our planet. The mantle is characterized by significantly higher temperatures and pressures than the Earth's crust and is the source of a wide arrange of common geological events, for instance plate tectonics, volcanism and earthquakes. None of these processes are fully understood nor predictable at the time this study has been carried out. The aim of this work is to create a better understanding of the high-pressure behavior of natural pyroxenes using an analogue of spodumene-type clinopyroxene with the chemical composition of $\text{LiScGe}_2\text{O}_6$. There is currently no established method to

predict the compression behavior of pyroxenes. There are already some models which describe the compression behavior of certain substances, like pyroxenes, but they lack in accuracy (Anderson and Nafe, 1965). Recent studies of Nestola et al. (2012) provided a new idea for a much more accurate model for predicting compression behavior but this model lacks in sufficient data points.

1.2 Subject of this study

The aim of this study is to create a wholesome understanding of the high-pressure behavior of the clinopyroxene with a general structure of $M1^{[6]}M2^{[6]}T_4O_6$ and the chemical composition of $LiScGe_2O_6$. This is achieved by using in-situ Raman spectroscopy and x-ray diffraction methods. The obtained data is set in context and compared to current data for better interpretation and extends the presented model by Nestola et al. (2012) and proves its higher accuracy.

2 Materials and methods

All methods and formulae described in this section assume ideal conditions, like perfect mechanics of the diffractometers or perfect crystals with no defects. Due to the limits of our current technology, perfect mechanics or defect-free crystals are not achievable. These imperfections do not invalidate the models and formulas. The deviations from the ideal models are represented as errors of measurements. All experiments were conducted at a constant temperature of 20°C.

2.1 Sample material

The $LiScGe_2O_6$ (*LSG*) crystals were synthesized by Günther Redhammer at the University of Salzburg. Most of the needle-like crystals exceed 250 μm in length and have an approximately quadratic cross-section with an edge length of 80 μm . All of them have at least two morphologically different crystal faces. They are

clear and transparent and show a hardly notice able shade of blue. For all experiments, the crystals were cut to a size of approximately $150 \times 50 \times 50 \mu\text{m}^3$.

2.2 The diamond-anvil cell

During all high-pressure experiments, an *Eidgenössische Technische Hochschule Zürich*-type diamond-anvil cell (*ETH-DAC*) (Miletich et al., 2000) was used. Because this work centers around the *ETH-DAC*, a short explanation about how it works will be given in the following paragraph.

The cell is build around its two parallel adjusted diamond anvils. These two diamonds terminate the top and bottom the sample-chamber space. The upper diamond of the *ETH-DAC* is mounted via s spring-leaf onto the backing plate, which is made out of beryllium for x-ray transparency. The backing plate has a hole in the middle. This allows optical access through the diamonds to the sample with incident and transmitted light microscopy. These components are fixed inside the so-called rocking-hemisphere which allows a parallel alignment of the two diamonds. The rocking-hemisphere rests inside the upper plate, where also the four screws for adjusting the rocking-hemisphere are located. The lower diamond is fixed in the same way as the upper diamond onto a beryllium backing-plate. This lower beryllium backing plate, which is designed the same way as the upper one, is placed inside a y-z-translation stage. The y-z direction is named with respect to the mounting position of the *ETH-DAC* inside a diffractometer. This stage assures that the two diamonds are congruent to each other. The stage rests inside the lower plate, which incorporates four screws for moving the y-z-stage. The lower and upper plate are plunged together with four guiding pins which are a part of the lower plate. The plates are fixed by two right-handed and two left-handed screws. The use of different-handed screws improves the handling of the *ETH-DAC* during preparation of experiments. These screws are also responsible for applying pressure to the sample-chamber.

The walls of the sample-chamber are defined by the gasket. The used gasket material was steel 1.6358. In this study, all gaskets were pre-indented to approximately

100 μm . This defines the initial height of the sample chamber. The diameter of the sample chamber is defined by a hole drilled with common means into the gasket, which was always 250 μm in this work. The gasket is positioned with plasticine inside the *ETH-DAC* and is later fixated by the diamond-anvils when the cell loading is complete.

The sample chamber is flooded with a pressure fluid. It converts the axial pressure generated by the diamonds to isostatic pressure onto the sample. A 4:1 methanol:ethanol mixture was used, which allows isostatic compression up to 10 GPa (Angel et al., 2007).

2.2.1 Used diamonds

The modular design of the *ETH-DAC* allows the use of different diamond-anvils according to the task at hand. For the isostatic-compression experiments, a brilliant-cut anvil was used due to its availability. For the high-pressure structure refinements, Boehler-Almax-cut anvils (Boehler and De Hantsetters, 2004) were used. Because of its proportions, this anvil does not need the beryllium back-plating and is thinner than the brilliant-cut anvil. These advantages reduce the amount of scattered x-rays and improves the intensity to background ratio. These properties improve the quality of the collected data. For a comparison of the properties of the used anvils, see Table 1.

Anvil	Weight [ct]	Height [mm]	Griddle	Table	Culet
Brilliant	0.09	1.40	3.00	2.80	0.60
Boehler-Almax	0.15	1.00	4.00	3.19	0.60

Table 1: List of the physical properties of the used diamond-anvils. All diamonds were natural 1A diamonds.

Mounting the sample crystal, ruby and quartz (see section 2.4) inside the sample chamber, filling the sample chamber with the pressure fluid and screwing the *DAC* plates together is called loading. Table 2 summarizes all used loadings and the properties of the contents of the *ETH-DAC*. For reference, a *LSG* crystal on a glass fiber was also measured. Two loadings for the x-ray compression study were

made because the pressure fluid got solid in the first loading. This solidification was probably due to the contamination of the used alcoholic agents with water. The unknown amount of water changed the desired ratio of methanol and ethanol which lead in combination with the additional water in the system to a lower solidification point of the pressure fluid than expected.

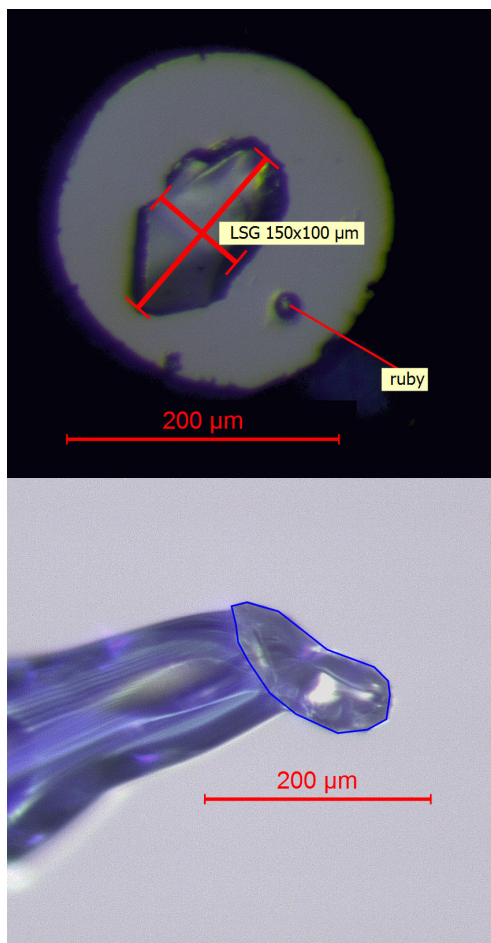
Image of loading	properties of loading
	<p>First loading</p> <ul style="list-style-type: none"> • Purpose: x-ray compression study • Pressure fluid: 4:1 = methanol:ethanol • Covered pressure: 0.02 to 3.56 GPa • Anvil: Brilliant <p>Second loading</p> <ul style="list-style-type: none"> • Purpose: x-ray and Raman compression study • Pressure fluid: 4:1 = methanol:ethanol • Covered pressure: 0.56 GPa to 4.99 GPa • Anvil: Brilliant

Continued on next page

Continued from last page

Image of loading

properties of loading



Third loading

- Purpose: Structure-refinement
- Pressure fluid:
4:1 = methanol:ethanol
- Covered pressure: 4.95 and
9.51 GPa
- Anvil: Boehler-Almax

Glass filament reference

- Purpose: Structure-refinement
- Covered pressure: 0 GPa

Table 2: Summary of all *ETH-DAC* loadings and their properties.

2.3 Raman spectroscopy

A Renishaw RM1000 spectrometer was used to obtain the pressure inside the *ETH-DAC* with the ruby R1 line. Raman-spectra from 0.0001 to 5.12 GPa were obtained using a Horiba Jobin Yvon LabRAM-HR 800 spectrometer. Table 3 summarizes the experimental setup for both instruments. If a phase-transition occurs, Raman bands would have joined in case of a symmetry increase or split in case of a symmetry decrease. This is a powerful and fast tool to see if a phase transition occurs and at which pressure. The obtained spectra were fitted with

PeakFit 4 and the Gauss-Lorentz-Area method.

	Laser [nm]	Lower limit	Upper limit	Time [s]
Renishaw	633	690 nm	700 nm	1
Horiba	532	60 cm ⁻¹	1200 cm ⁻¹	180

Table 3: Experimental setup for Raman-spectrometers during pressure acquisition and compression study. the hole was set to 100 in both cases.

2.4 Pressure gauge

Determination of the correct pressure with a high precision is a crucial part for high-pressure studies. For a first approximation of the pressure, the shift of the ruby R1 luminescence line was used (Mao et al., 1986). This method allows a quick determination and adjustment of the pressure. The obtained Raman spectra and structure refinements relied on this method. In order to achieve a more precise determination of pressure, a quartz crystal was used (Angel et al., 1997) with a (*hk0*)-cut alongside *LSG*. The lattice parameters of quartz were obtained with x-rays in the same way as the lattice parameters of *LSG*. By using these lattice parameters and the equation of state (see section 2.5) of quartz the pressure can be easily calculated. Because the lattice parameters can be obtained with a much higher precision than the shift of the ruby luminescence lines, the determination of the pressure with quartz is more accurate.

2.5 Equation-of-state

For the description of the lattice compression of a crystal, a so called equation-of-state (*EoS*) is used. Depending on the intended use, a plethora of *EoS* exist (Angel et al., 2000). A typical and common *EoS* for the description of isothermal compression is the fourth-order Birch-Murnaghan equation.

$$P(V) = 3K_0 f_E (1 + 2f_E)^{\frac{5}{2}} \times \left\{ 1 + \frac{3}{2}(K' - 4)f_E + \frac{3}{2} \left[K_0 K'' + (K' - 4)(K' - 3) + \frac{35}{9} \right] f_E^2 \right\} \quad (1)$$

$$f_E = \frac{1}{2} \left[\left(\frac{V_0}{V} \right)^{\frac{2}{3}} - 1 \right] \quad (2)$$

$$K'' = \frac{-1}{K_0} \left[(3 - K')(4 - K') + \frac{35}{9} \right] \quad (3)$$

with

- P ... pressure
- V ... current volume
- K_0 ... bulk modulus
- K' ... first derivative $\frac{\delta K}{\delta P}$
- K'' ... second derivative $\frac{\delta^2 K}{\delta P^2}$
- f_E ... Euler strain
- V_0 ... volume at room-conditions

When equation 1 is resolved with equation 2 and equation 3, the results is a third-order Birch-Murnaghan:

$$P(V) = \left(\frac{3}{2} K_0 \right) \left[\left(\frac{V_0}{V} \right)^{\frac{7}{3}} - \left(\frac{V_0}{V} \right)^{\frac{5}{3}} \right] \times \left\{ 1 + \left[\frac{3}{4} (K' - 4) \right] \left[\left(\frac{V_0}{V} \right)^{\frac{2}{3}} - 1 \right] \right\} \quad (4)$$

2.6 X-ray diffractometry

For this work, two different types and three different instruments were used. The first type was a STOE StadiVari single crystal four-circle diffractometer with an open Euler cradle. It was used for the data collection for the structure-refinement and determination of the UB matrix. It was equipped with a micro-focus x-ray source with Mo $\lambda_{K\alpha} = 0.7093 \text{ \AA}$ radiation. The incident beam was chroma-tized with a point-focusing multi-layer optics and the diffracted beam was mea-sured with a Dectris PILATUS 300K area detector. For the experimental setup see table 4. The X-Area (version 8/13) software suit by STOE was used to

control the diffractometer, correction calculations and to obtain the UB matrix. The SHELX program suit (version 2014/3) (Sheldrick, 1997) was used for the structure-refinement.

The second type was a single crystal four-circle diffractometer with a closed Euler cradle and a scintillation counter. The lattice parameters during the compression were measured with this type. Due to time constraints, two different instruments were employed, a STOE AED 2 and a Huber 5042. The STOE AED 2 was equipped with a conventional fine-focusing x-ray source with Mo $\lambda_{K\alpha} = 0.7093$ Å radiation. The incident beam was chromatized with a graphite(002) monochromator crystal. The Huber 5042 was equipped with a conventional normal-focusing x-ray source with Mo $\lambda_{K\alpha} = 0.7093$ Å radiation and was not equipped with a monochromator. For the compression study, the *8-position-centering* method (Hamilton, 1974) was used. This method eliminates mechanical aberrations of the diffractometer by measuring a Friedl-pair of reflections in eight different diffractometer angle settings. About twenty unique reflections were used for each pressure point to determine the lattice parameters. This number is constrained because of the opening angle by the *ETH-DAC* and the dampening of the incident and refracted beam by the diamonds. See table create table! for the diffractometer settings for the measurement of a single reflection. The SINGLE software (Angel and Finger, 2010) was used to control both diffractometers and to calculate the lattice parameters with the least-squares method.

For visualizing crystal structures, ATOMS 6.2 was used. All plots were created in Origin 9.1.

Pressure	0.0001 GPa	4.95 GPa	9.51 GPa
Crystal data			
Spacegroup	$P2_1/c$	$P2_1/c$	$P2_1/c$
a [Å]	9.9999(8)	9.8454(6)	9.697(9)
b [Å]	9.1040(2)	8.9535(7)	8.829(4)
c [Å]	5.4610(2)	5.363(9)	5.295(5)
β [°]	109.240(2)	108.638(9)	108.17(6)
V [Å ³]	469.61(11)	447.9(7)	429.5(5)
Z	4	4	4
Data collection			
# measured reflections	27757	9338	9492
Rejected	679	486	510
Unique reflections	3091	504	483
Max. 2θ [°]	82.40	69.86	69.35
Range of hkl	$-15 \leq h \leq 18$	$-13 \leq h \leq 12$	$-11 \leq h \leq 11$
	$-16 \leq k \leq 16$	$-13 \leq k \leq 10$	$-14 \leq k \leq 10$
	$-10 \leq l \leq 10$	$-6 \leq l \leq 6$	$-7 \leq l \leq 7$
Structure refinement			
$R1(F_o > 4\sigma)^1$	0.0215	0.0380	0.0391
$wR2^2$	0.0487	0.995	0.0956
Goof ³	0.950	1.213	1.229
Parameters refined	87	52	52

Table 4: Experimental details of the crystal lattices, intensity data collections and structure refinements. Both α and γ are constraint to 90°.

$$^1R1 = \sum ||F_o| - |F_c|| / \sum |F_o|,$$

$$^2wR2 = \left\{ \frac{\sum [w(F_o^2 - F_c^2)^2]}{\sum [w(F_o^2)^2]} \right\}^{\frac{1}{2}},$$

$$^3\text{Goof} = \left\{ \frac{\sum [w(F_o^2 - F_c^2)^2]}{(n - p)} \right\}^{\frac{1}{2}}$$

where n = number of reflections and p = total number of parameters refined

3 Results

The following section presents all obtained data. They are discussed in the following section. All graphs include x- and y-error-bars but most of the time they are within symbol range.

3.1 High-pressure Raman spectra

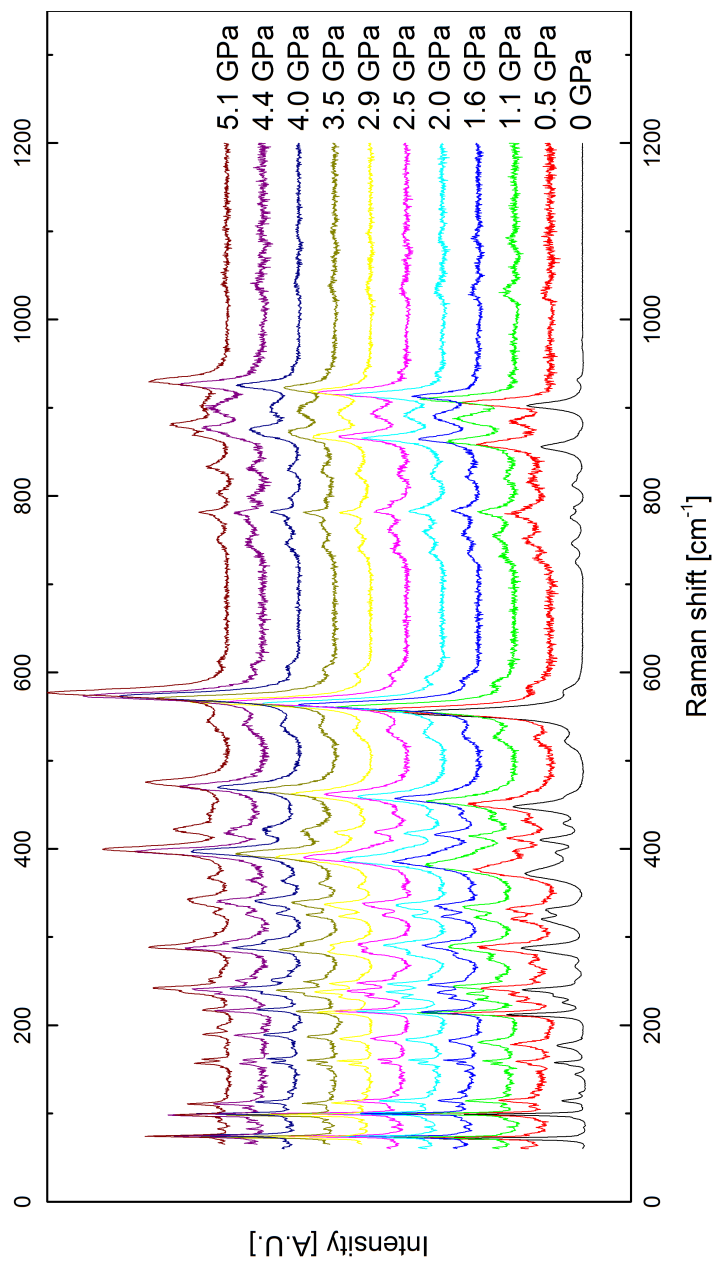


Figure 1: Obtained Raman spectra at different pressures. The increased noise and additional above 0 GPa are related to the pressure fluid.

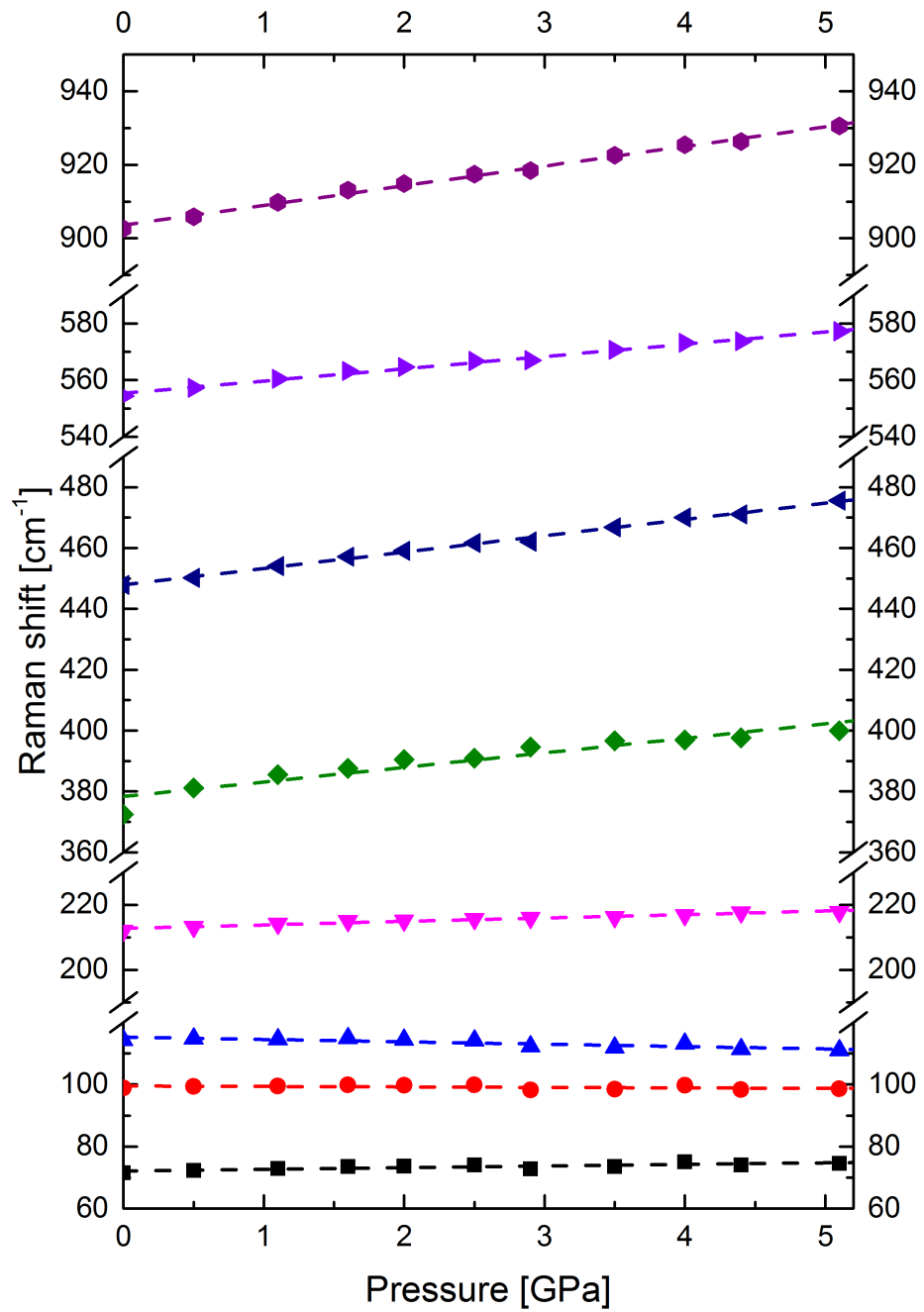


Figure 2: Shift of selected Raman-bands

3.2 Crystallography

	Parameter	0.0001 GPa	4.95 GPa	9.51 GPa
GeA	<i>x</i>	0.94985(2)	0.9494(3)	0.9492(3)
	<i>y</i>	0.16091(2)	0.16009(9)	0.15950(9)
	<i>z</i>	0.20386(2)	0.1949(5)	0.1888(4)
	U_{iso}	0.00514(3)	0.0081(13)	0.0118(13)
GeB	<i>x</i>	0.55445(2)	0.5585(2)	0.5608(3)
	<i>y</i>	0.16320(2)	0.16443(9)	0.16526(9)
	<i>z</i>	0.24412(2)	0.2398(4)	0.2374(4)
	U_{iso}	0.00503(3)	0.0090(14)	0.0121(13)
Li	<i>x</i>	0.7451(4)	0.742(4)	0.738(5)
	<i>y</i>	0.0096(4)	0.0111(19)	0.0103(18)
	<i>z</i>	-0.2224(7)	-0.217(8)	-0.213(7)
	U_{iso}	0.0201(6)	0.018(4)	0.016(4)
Sc	<i>x</i>	0.25101(2)	0.2509(4)	0.2513(5)
	<i>y</i>	0.35186(2)	0.35133(16)	0.35107(16)
	<i>z</i>	0.21971(4)	0.2111(8)	0.2059(7)
	U_{iso}	0.00507(4)	0.0060(4)	0.0054(4)
OA1	<i>x</i>	0.88205(12)	0.8846(16)	0.8852(18)
	<i>y</i>	-0.01238(11)	-0.0164(7)	-0.0187(6)
	<i>z</i>	0.1908(2)	0.195(3)	0.193(3)
	U_{iso}	0.01086(16)	0.0103(13)	0.0093(13)

Continued on next page

Continued from last page

	Parameter	0.0001 GPa	4.95 GPa	9.51 GPa
OA2	<i>x</i>	1.13493(10)	1.1352(18)	1.1363(18)
	<i>y</i>	0.17099(10)	0.1685(6)	0.1673(6)
	<i>z</i>	0.32225(18)	0.313(3)	0.307(3)
	U_{iso}	0.00640(13)	0.0082(13)	0.0070(12)
OA3	<i>x</i>	0.87997(11)	0.8775(15)	0.8733(17)
	<i>y</i>	0.28419(12)	0.2867(7)	0.2880(7)
	<i>z</i>	0.37771(18)	0.364(3)	0.355(2)
	U_{iso}	0.00961(15)	0.0092(13)	0.0097(13)
OB1	<i>x</i>	0.63221(11)	0.6340(16)	0.6320(17)
	<i>y</i>	0.00443(11)	0.0074(7)	0.0089(6)
	<i>z</i>	0.39189(19)	0.405(3)	0.411(2)
	U_{iso}	0.00863(15)	0.0105(13)	0.0077(12)
OB2	<i>x</i>	0.36836(10)	0.3730(18)	0.3712(18)
	<i>y</i>	0.16845(10)	0.1683(6)	0.1675(6)
	<i>z</i>	0.12085(17)	0.118(3)	0.111(3)
	U_{iso}	0.00642(13)	0.0092(13)	0.0071(12)
OB3	<i>x</i>	0.60936(11)	0.6151(16)	0.6146(17)
	<i>y</i>	0.19186(11)	0.1826(7)	0.1770(6)
	<i>z</i>	-0.02956(18)	-0.040(3)	-0.050(2)
	U_{iso}	0.00856(15)	0.0092(13)	0.0066(12)

Table 5: Change of atomic coordinates and isotropic displacement parameters with pressure. All atoms have a Wyckoff letter of $4e$ and site-symmetry of 1 .

	Parameter	0.0001 GPa	4.95 GPa	9.51 GPa
GeA	U ₁₁	0.00415(6)	0.013(3)	0.022(3)
	U ₂₂	0.00657(6)	0.0075(4)	0.0062(4)
	U ₃₃	0.00504(5)	0.005(3)	0.013(2)
	U ₂₃	-0.00013(3)	0.0001(5)	-0.0008(5)
	U ₁₃	0.00198(4)	0.005(3)	0.013(2)
	U ₁₂	-0.00111(4)	-0.0009(5)	-0.0020(6)
GeB	U ₁₁	0.00416(6)	0.015(3)	0.024(3)
	U ₂₂	0.00619(6)	0.0067(4)	0.0062(4)
	U ₃₃	0.00486(5)	0.008(3)	0.0121(19)
	U ₂₃	0.00021(3)	-0.0003(5)	-0.0002(5)
	U ₁₃	0.00166(4)	0.007(3)	0.014(2)
	U ₁₂	0.00100(4)	0.0000(6)	0.0011(6)

Table 6: Anisotropic displacement parameters of germanium at different pressures.

	U ₁₁	U ₂₂	U ₃₃	U ₂₃	U ₁₃	U ₁₂
Sc	0.00454(8)	0.00577(8)	0.00520(7)	-0.00007(6)	0.00204(6)	0.00010(6)
OA1	0.0108(4)	0.0081(4)	0.0154(4)	-0.0005(3)	0.0065(3)	-0.0040(3)
OA2	0.0045(3)	0.0084(3)	0.0062(3)	0.0005(3)	0.0017(2)	-0.0004(3)
OA3	0.0076(4)	0.0150(4)	0.0060(3)	-0.0025(3)	0.0020(3)	0.0019(3)
OB1	0.0096(4)	0.0081(3)	0.0091(3)	0.0024(3)	0.0042(3)	0.0042(3)
OB2	0.0041(3)	0.0084(3)	0.0065(3)	-0.0002(2)	0.0014(2)	0.0009(3)
OB3	0.0087(4)	0.0112(4)	0.0071(3)	0.0027(3)	0.0044(3)	0.0013(3)

Table 7: Anisotropic displacement parameters of scandium and oxygen at ambient pressure.

	0.0001 GPa	4.95 GPa	9.51 GPa
GeA – OA1	1.7094(10)	1.703(7)	1.694(7)
GeA – OA2	1.7499(10)	1.736(17)	1.721(18)
GeA – OA3	1.7569(10)	1.739(6)	1.736(6)
GeA – OA3 ⁱ	1.7580(9)	1.752(14)	1.748(13)
GeB – OB1	1.7123(10)	1.702(11)	1.680(10)

Continued on next page

Continued from last page

	0.0001 GPa	4.95 GPa	9.51 GPa
GeB – OB2	1.7583(10)	1.732(17)	1.744(17)
GeB – OB3 ⁱⁱ	1.7672(10)	1.768(8)	1.760(10)
GeB – OB3	1.7733(9)	1.776(11)	1.764(6)
Li – OA1	2.230(4)	2.22(5)	2.18(4)
Li – OB1 ⁱⁱⁱ	2.036(3)	1.97(5)	1.93(4)
Li – OA2 ^{iv}	2.207(4)	2.17(2)	2.14(2)
Li – OB2 ^v	2.153(4)	2.13(2)	2.06(2)
Li – OA3 ⁱ	2.271(4)	2.21(3)	2.17(3)
Li – OB3	2.578(4)	2.362(18)	2.235(19)
Sc – OA1 ^{vi}	1.9912(10)	1.967(8)	1.953(9)
Sc – OB1 ^{vi}	2.0330(10)	2.018(7)	2.012(8)
Sc – OA2 ^{vii}	2.1076(9)	2.082(19)	2.056(16)
Sc – OB2 ⁱⁱ	2.1252(9)	2.135(19)	2.092(16)
Sc – OA2 ^{viii}	2.1911(10)	2.161(7)	2.130(8)
Sc – OB2	2.2077(9)	2.184(7)	2.149(8)
GeA – GeA	3.1763(9)	3.130(12)	3.092(17)
GeB – GeB	3.1555(8)	3.090(11)	3.041(15)

Table 8: Selected inter-atomic distances in Å. Symmetry code: ⁱ x, -y+1/2, z-1/2; ⁱⁱ x, -y+1/2, z+1/2; ⁱⁱⁱ x, y, z-1; ^{iv} -x+2, -y, -z; ^v -x+1, -y, -z; ^{vi} -x+1, y+1/2, -z+1/2; ^{vii} x-1, -y+1/2, z-1/2; ^{viii} x-1, y, z

	0.0001 GPa	4.95 GPa	9.51 GPa
OA1 – GeA – OA3 ⁱ	101.56(5)	102.9(6)	102.9(6)
OA3 – GeA – OA3	105.66(4)	104.5(6)	103.2(6)
OA2 – GeA – OA3	109.10(5)	109.8(6)	111.1(6)
OA2 – GeA – OA3	112.23(4)	113.3(5)	114.2(5)
OA1 – GeA – OA3	112.91(5)	113.0(3)	112.6(3)
OA1 – GeA – OA2	114.86(5)	112.9(6)	112.3(6)
OB2 – GeB – OB3	104.81(4)	107.7(5)	103.5(6)

Continued on next page

Continued from last page

	0.0001 GPa	4.95 GPa	9.51 GPa
OB2 – GeB – OB3	107.05(5)	104.9(7)	107.2(5)
OB1 – GeB – OB3	107.63(5)	107.4(7)	109.7(4)
OB1 – GeB – OB3 ⁱⁱ	108.21(5)	108.3(4)	108.3(6)
OB3 – GeB – OB3 ⁱⁱ	111.63(4)	112.1(3)	113.4(3)
OB1 – GeB – OB2	117.53(5)	116.5(5)	114.8(5)
OA1 – Li – OA3 ⁱ	73.29(11)	75.2(14)	76.3(14)
OA3 ⁱ – Li – OB3	73.75(11)	75.6(7)	76.5(7)
OB2 ⁱⁱⁱ – Li – OA1	82.63(12)	83.3(12)	83.1(10)
OA1 – Li – OB3	82.80(12)	85.5(11)	87.8(10)
OB2 ⁱⁱⁱ – Li – OA ^v	83.01(14)	83.2(7)	83.2(7)
OB1 ^{iv} – Li – OA2 ^v	83.58(13)	84.5(11)	84.8(10)
OA1 – Li – OA2 ^v	88.89(13)	85.9(14)	84.2(15)
OB2 ⁱⁱⁱ – Li – OB3	89.23(12)	89.9(7)	91.1(9)
OB1 ^{iv} – Li – OB2 ⁱⁱⁱ	95.15(15)	95.3(17)	96.9(17)
OB1 ^{iv} – Li – OB3	104.52(14)	104.1(17)	103.3(17)
OA2 ^v – Li – OA3 ⁱ	110.32(15)	107.9(13)	106.1(15)
OB1 ^{iv} – Li – OA3 ⁱ	110.54(16)	108.1(11)	105.5(9)
OB2 ⁱⁱⁱ – Li – OA3 ⁱ	151.87(17)	154.8(19)	156.3(17)
OA2 ^v – Li – OB3	169.30(17)	169.5(16)	170.7(15)
OA1 – Li – OB1 ^{iv}	172.4(2)	170.4(11)	169(13)
OA2 ^{vi} – Sc – OB2	80.22(4)	82.1(6)	81.7(5)
OA2 ^{vii} – Sc – OB2 ⁱⁱ	80.22(4)	81.3(6)	81.2(6)
OA2 ^{vii} – Sc – OB2	82.13(4)	82.1(3)	81.4(3)
OB1 ^{viii} – Sc – OA2 ^{vi}	86.24(4)	85.3(5)	84.9(5)
OA1 ^{viii} – Sc – OA2 ^{viii}	87.17(4)	86.3(3)	85.7(3)
OA1 ^{viii} – Sc – OB2 ⁱⁱ	89.28(4)	89.7(5)	88.3(5)
OB2 – Sc – OB2 ⁱⁱ	91.66(3)	90.3(6)	90.9(6)
OA2 ^{vii} – Sc – OA2 ^{vi}	91.76(3)	92.1(6)	92.5(6)
OB1 ^{viii} – Sc – OB2	92.26(4)	92.6(3)	92.9(3)

Continued on next page

Continued from last page

	0.0001 GPa	4.95 GPa	9.51 GPa
OA1 ^{viii} – Sc – OA2 ^{vi}	97.38(4)	96.9(6)	97.8(6)
OA1 ^{viii} – Sc – OB1 ^{viii}	98.38(4)	99.0(3)	100.0(3)
OB1 ^{viii} – Sc – OB2 ⁱⁱ	101.07(4)	100.6(6)	100.7(6)
OA1 ^{viii} – Sc – OB2	168.94(4)	168.3(3)	167.1(3)
OA2 ^{viii} – Sc – OB2 ⁱⁱ	169.34(4)	170.3(2)	170.9(2)
OB1 ^{viii} – Sc – OA2 ^{vii}	174.29(4)	174.3(2)	174.3(2)
GeA – OA3 – GeA	129.29(6)	127.3(9)	125.2(9)
GeB – OB3 – GeB	126.04(6)	121.2(4)	119.3(4)
OA3 – OA3 – OA3	154.32(4)	152.5(6)	151.6(6)
OB3 – OA3 – OB3	137.63(5)	131.6(7)	128.1(5)

Table 9: Selected inter-atomic angles in °. Symmetry code: ⁱ x, -y+1/2, z-1/2; ⁱⁱ x, -y+1/2, z+1/2 ⁱⁱⁱ -x+1, -y, -z; ^{iv} x, y, z-1; ^v -x+2, -y, -z; ^{vi} x-1, -y+1/2, z-1/2; ^{vii} x-1, y, z ^{viii} -x+1, y+1/2, -z+1/2

	Parameter	0.0001 GPa	4.95 GPa	9.51 GPa
GeA	BLD _{tet}	0.98(10)	0.85(11)	1.00(11)
	BAV _{tet}	3.6(5)	3.4(5)	3.8(5)
GeB	BLD _{tet}	1.15(10)	1.58(12)	1.64(11)
	BAV _{tet}	3.1(5)	2.9(5)	2.9(5)
Li	BLD _{oct}	3.1(10)	3.3(11)	2.8(11)
	BAV _{oct}	11.4(13)	10.4(12)	9.9(12)
Sc	BLD _{oct}	5.3(4)	4.0(6)	3.9(6)
	BAV _{oct}	6.2(4)	6.0(1)	6.6(1)

Table 10: Distortion parameters of coordination polyhedrons after Renner and Lehmann (1986) where BLD describes the bond-length distortion and BAV the bond-angle variance. All values are in %.

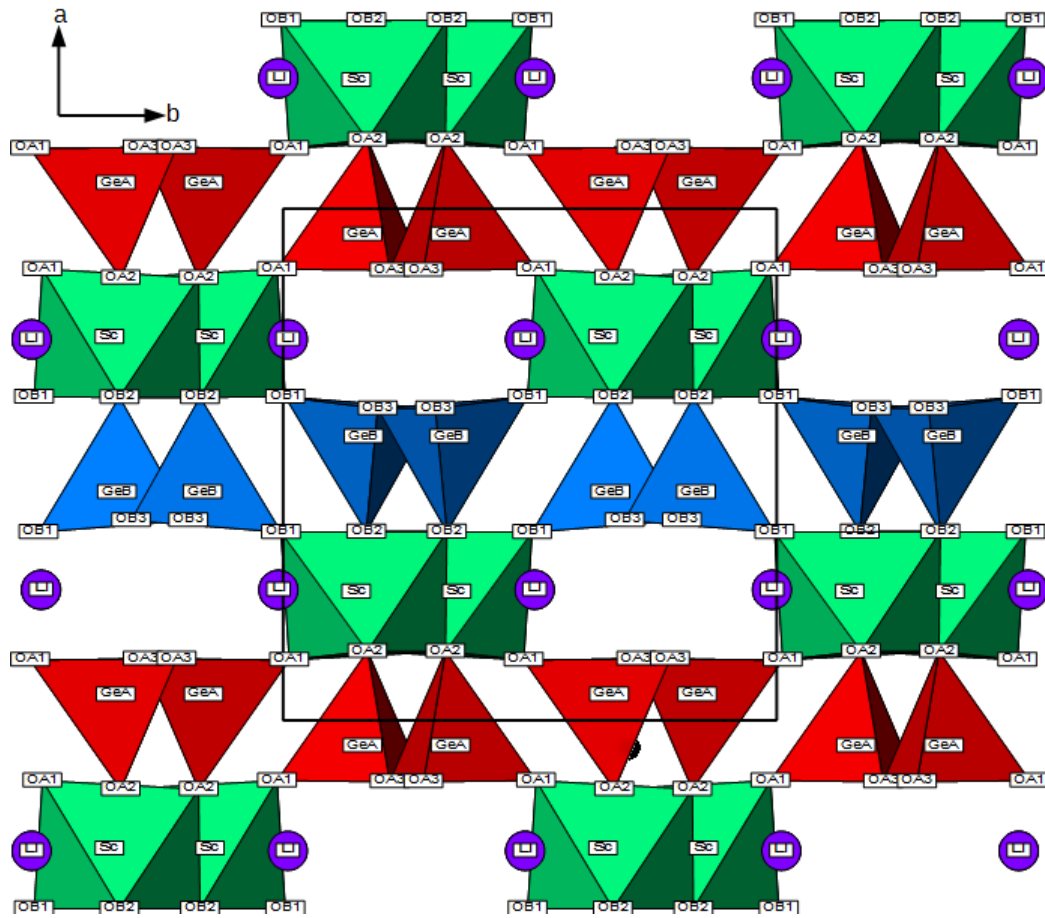


Figure 3: Crystal structure along [001] at ambient conditions. For better visibility were Li-polyhedrons omitted.

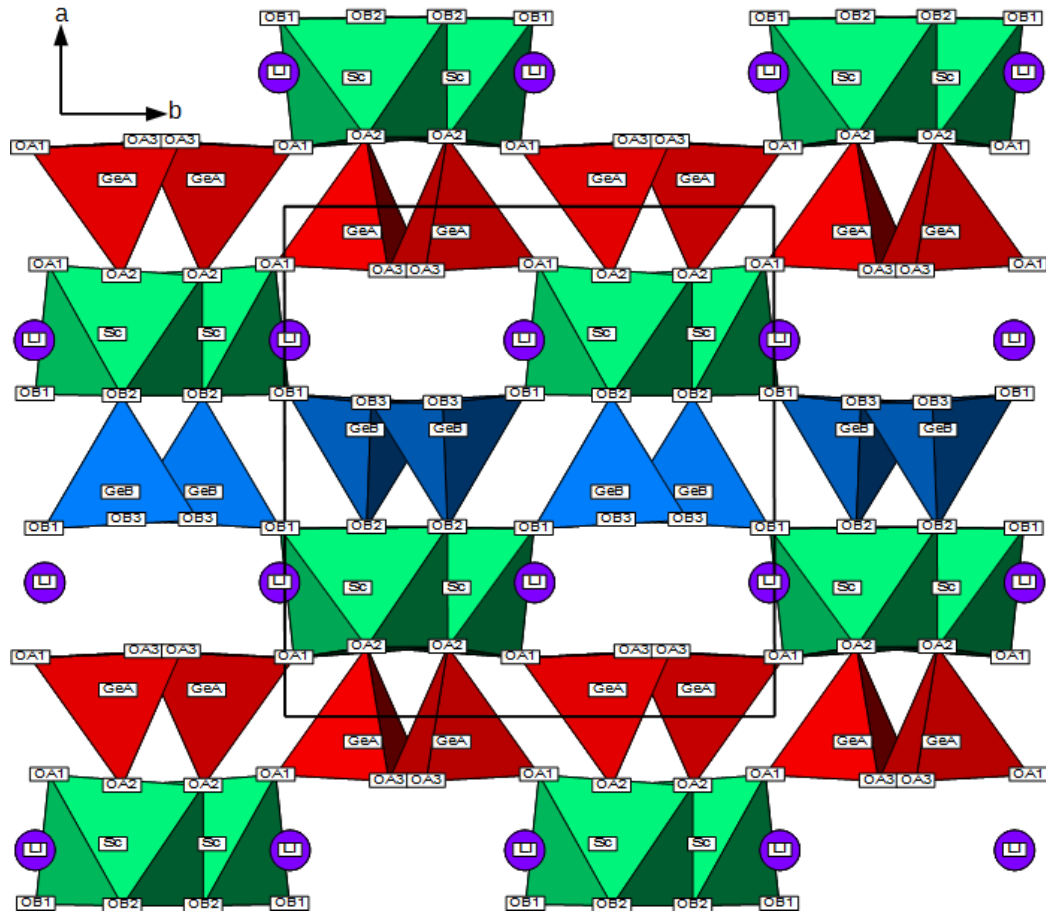


Figure 4: Crystal structure along [001] at 9.51 GPa. For better visibility were Li-polyhedrons omitted.

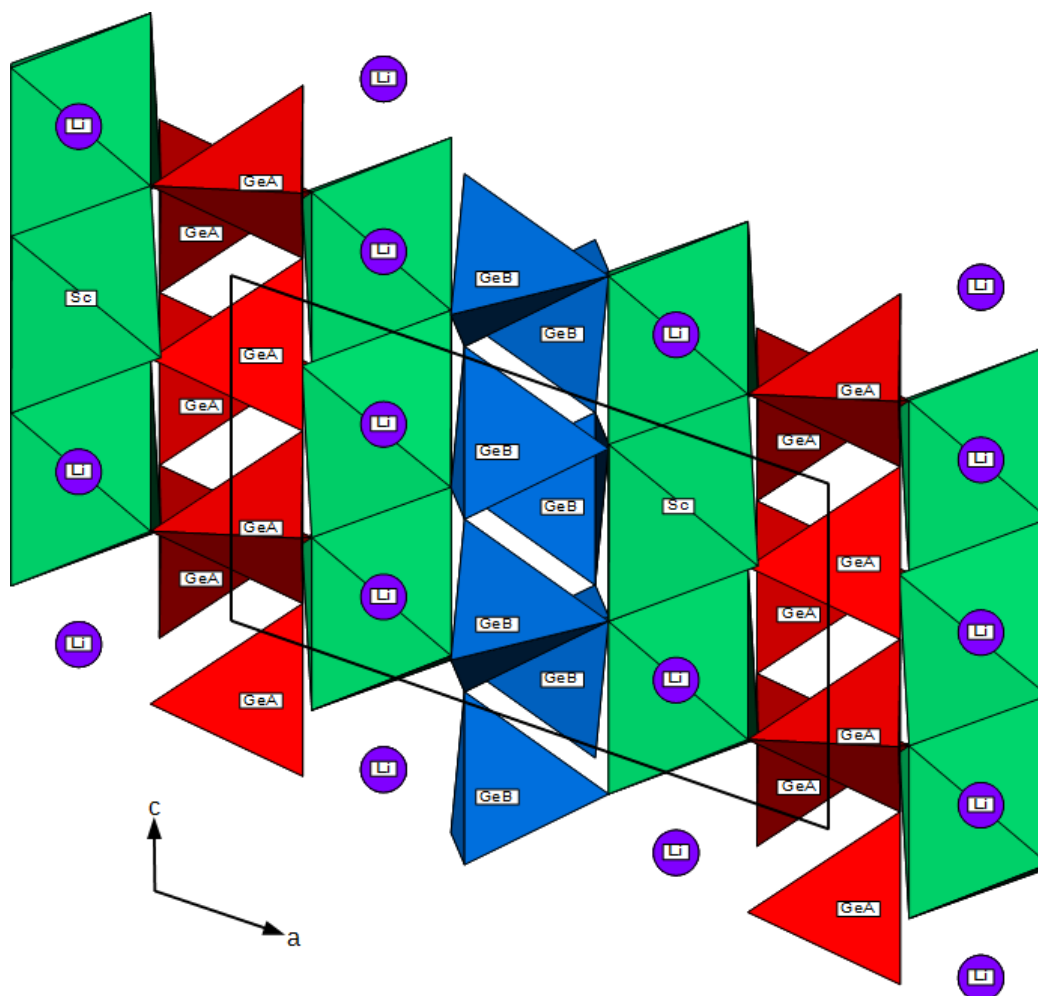


Figure 5: Crystal structure along [010] at ambient conditions. For better visibility were Li-polyhedrons omitted.

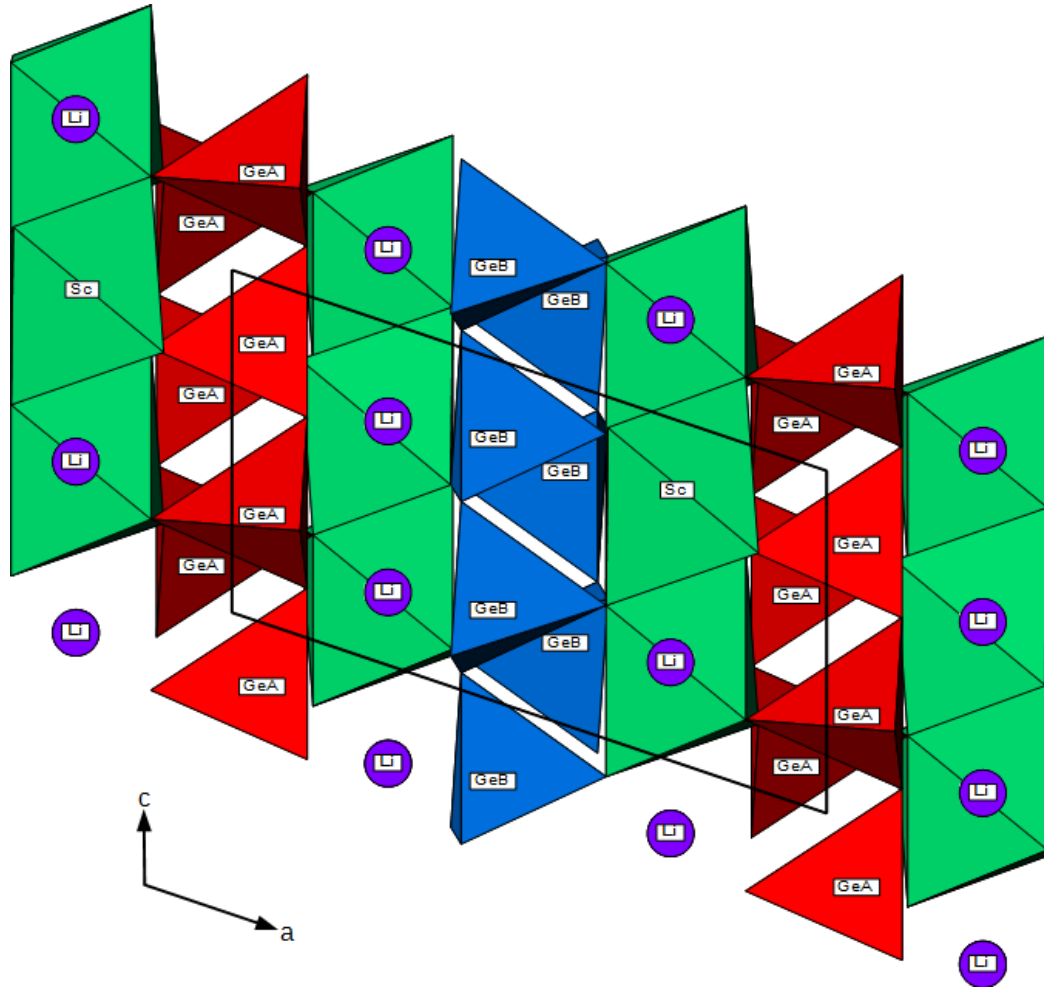


Figure 6: Crystal structure along [010] at 9.51 GPa. For better visibility were Li-polyhedrons omitted.

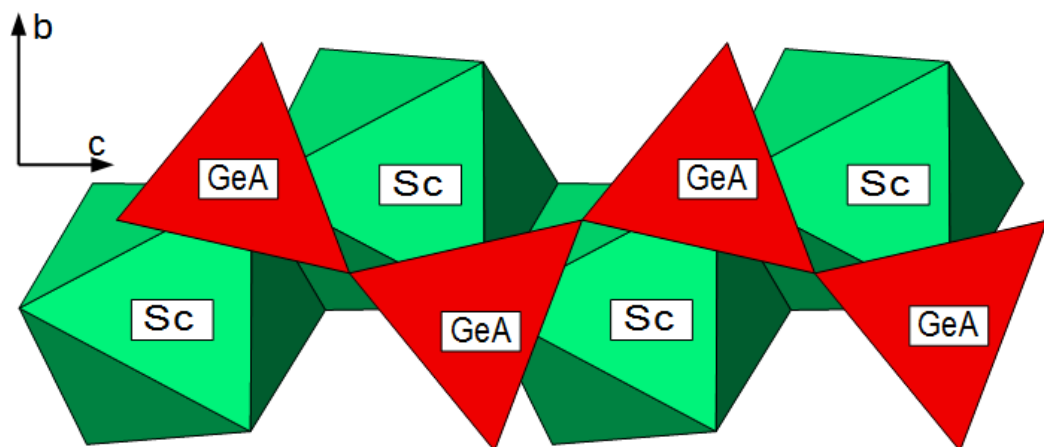


Figure 7: Germanate tetrahedral A-chain along [100] at ambient conditions.

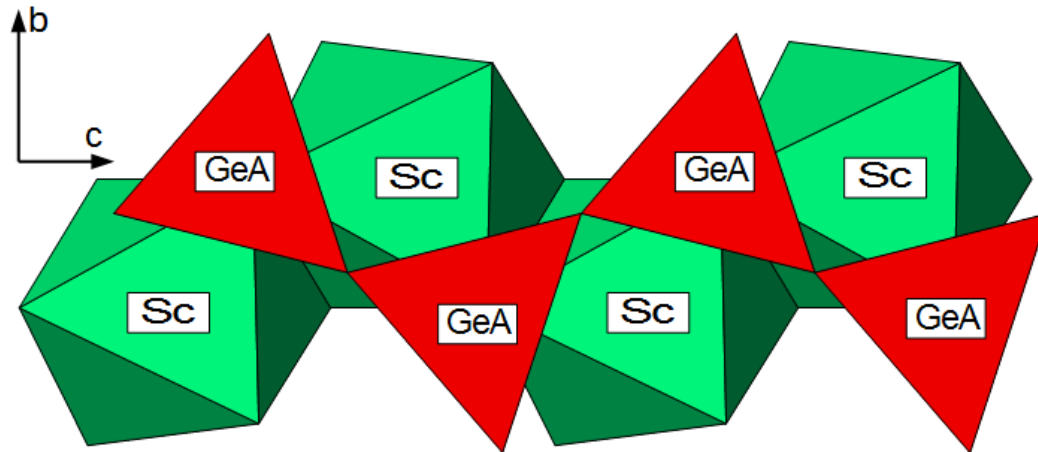


Figure 8: Germanate tetrahedral A-chain along [100] at 9.51 GPa.

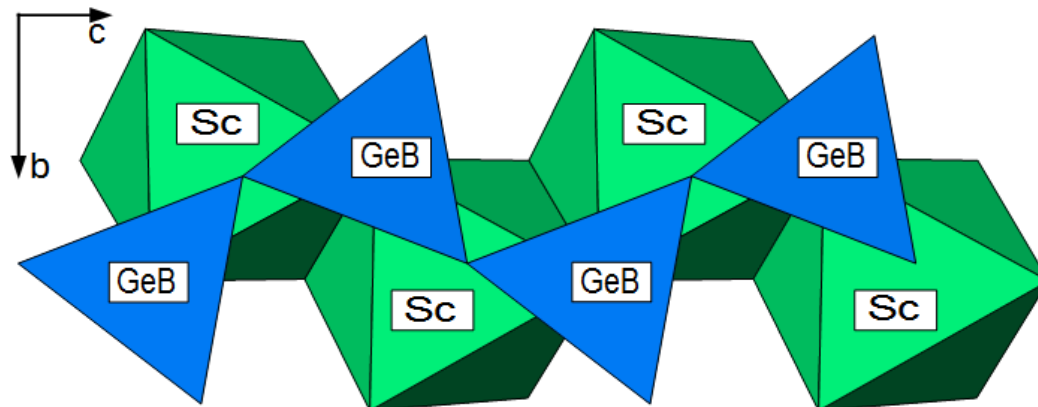


Figure 9: Germanate tetrahedral B-chain along [100] at ambient conditions.

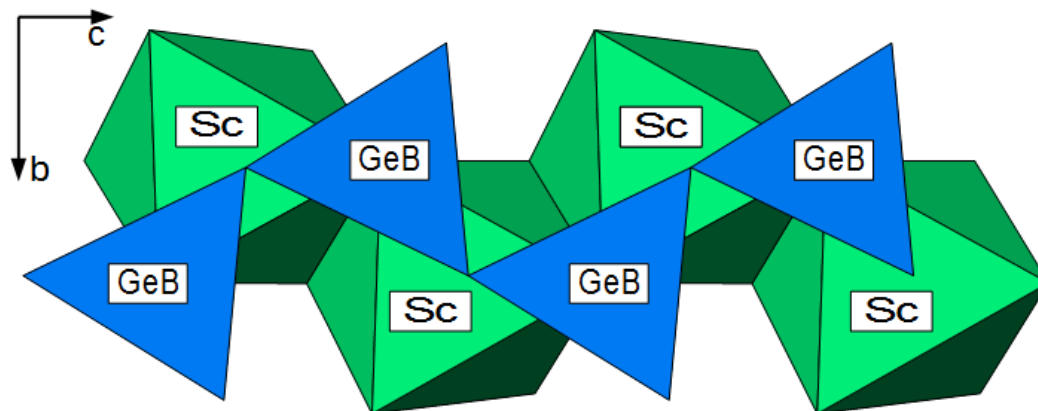


Figure 10: Germanate tetrahedral B-chain along [100] at 9.51 GPa.

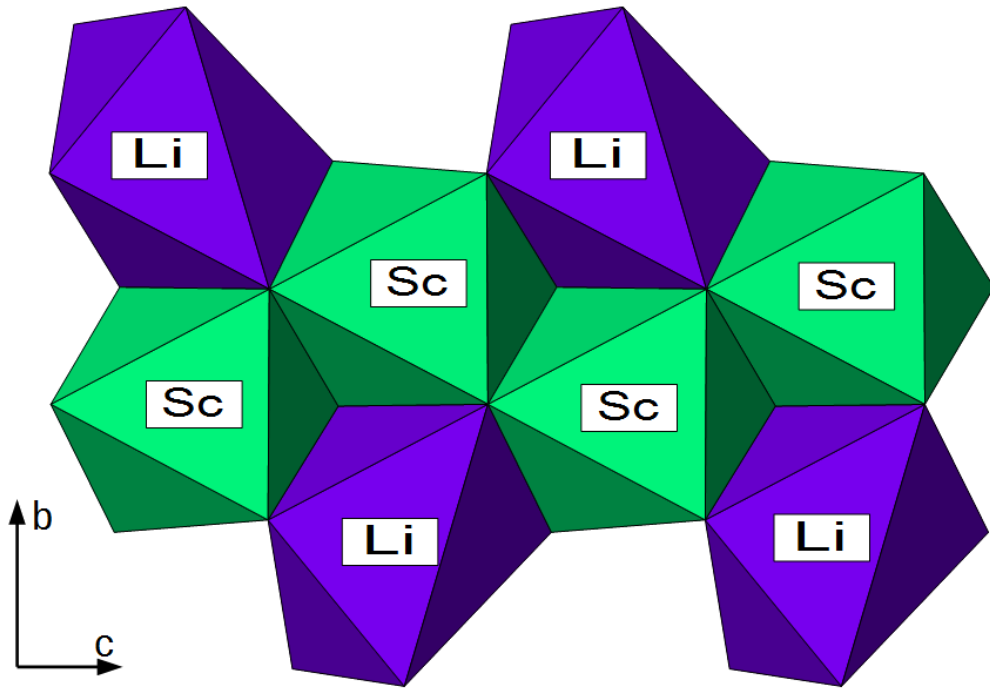


Figure 11: Octahedral layer along [100] at ambient conditions.

3.3 Isothermal compression

Point	P [GPa]	V [\AA^3]	a [\AA]	b [\AA]	c [\AA]	β [$^\circ$]
P0	0.0001	469.47(13)	9.9999(8)	9.1040(2)	5.4610(2)	109.240(2)
P1	0.021(7)	469.41(13)	9.9993(19)	9.1039(6)	5.4612(8)	109.228(18)
P2	0.032(11)	469.48(12)	10.0001(18)	9.1042(6)	5.4611(8)	109.219(17)
P3	0.133(9)	468.76(11)	9.9939(17)	9.1002(6)	5.4582(8)	109.209(16)
P4	0.564(9)	466.71(10)	9.9765(8)	9.0872(6)	5.4498(7)	109.159(11)
P5	0.802(8)	465.30(13)	9.9664(16)	9.0793(5)	5.4430(7)	109.141(15)
P6	1.138(9)	463.6(13)	9.9547(19)	9.0684(7)	5.4353(8)	109.118(18)
P7	1.577(8)	462.14(14)	9.9418(9)	9.0594(6)	5.4302(11)	109.106(14)
P8	1.665(11)	461.3(2)	9.9336(17)	9.0543(10)	5.4259(16)	109.023(2)
P9	2.043(8)	459.48(10)	9.9234(14)	9.0422(6)	5.4168(6)	109.030(13)
P10	2.100(3)	458.76(5)	9.9155(3)	9.0373(2)	5.4156(4)	109.030(5)
P11	2.162(16)	458.86(10)	9.9157(16)	9.0390(6)	5.4142(7)	108.985(14)
P12	2.563(15)	456.84(9)	9.9019(14)	9.0228(6)	5.4063(7)	108.950(13)
P13	3.561(11)	452.48(12)	9.870(2)	8.9937(6)	5.3868(9)	108.877(18)
P14	3.784(12)	451.44(9)	9.8601(6)	8.9874(4)	5.3846(7)	108.897(9)
P15	4.989(12)	446.99(9)	9.8241(8)	8.9562(5)	5.3661(7)	108.788(10)

Table 11: Experimental results after least-squares-refinement for lattice parameters at specific pressures. Both α and γ are constraint to 90° .

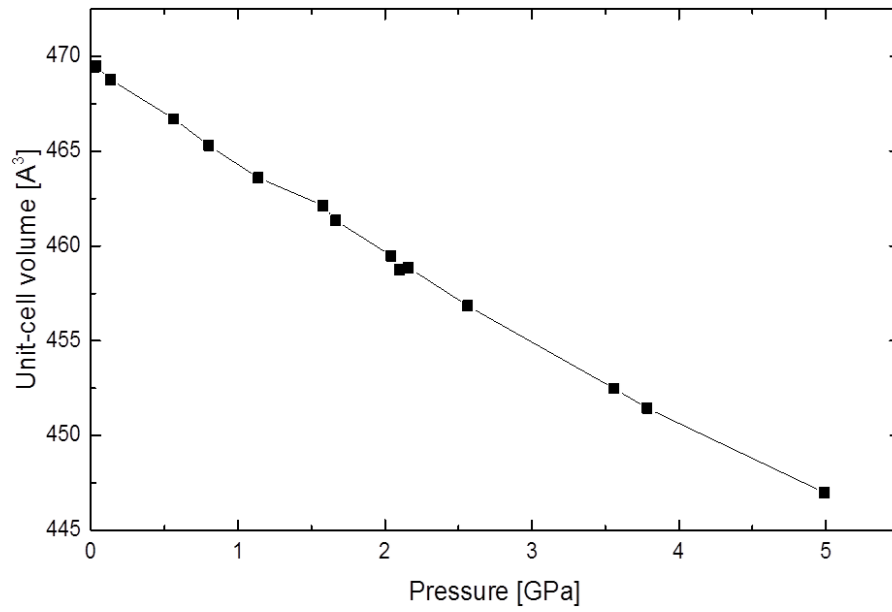


Figure 12: Compression of the unit-cell volume.

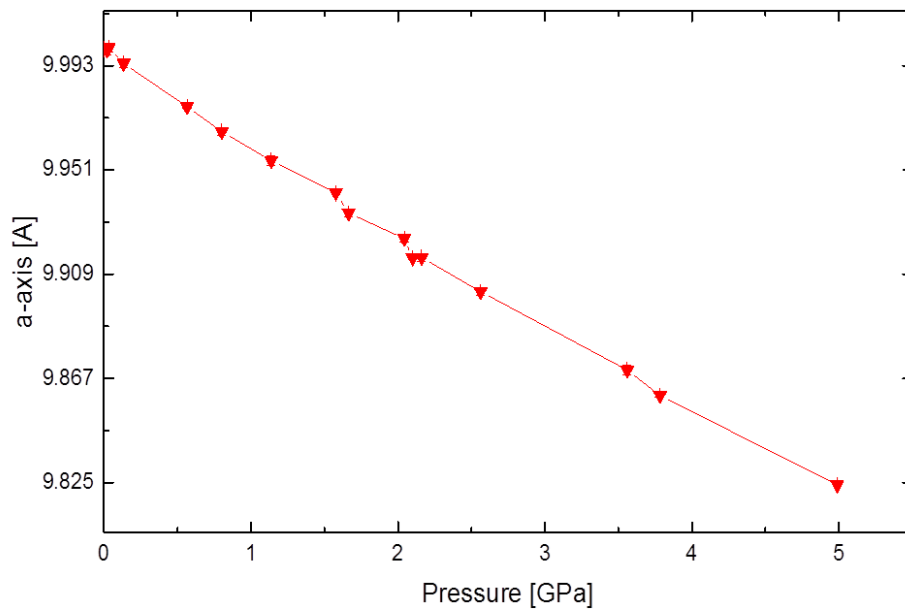


Figure 13: Compression of the a-axis.

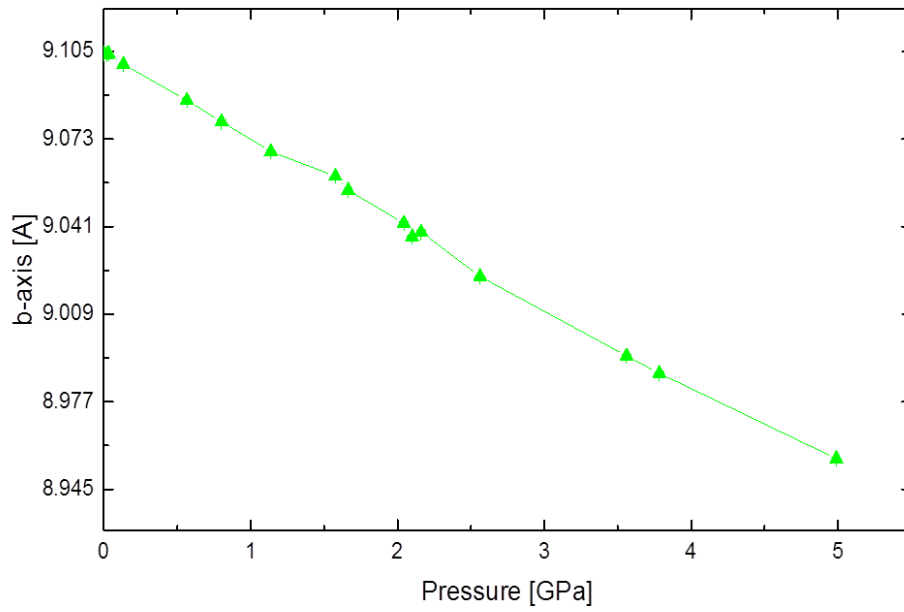


Figure 14: Compression of the b-axis.

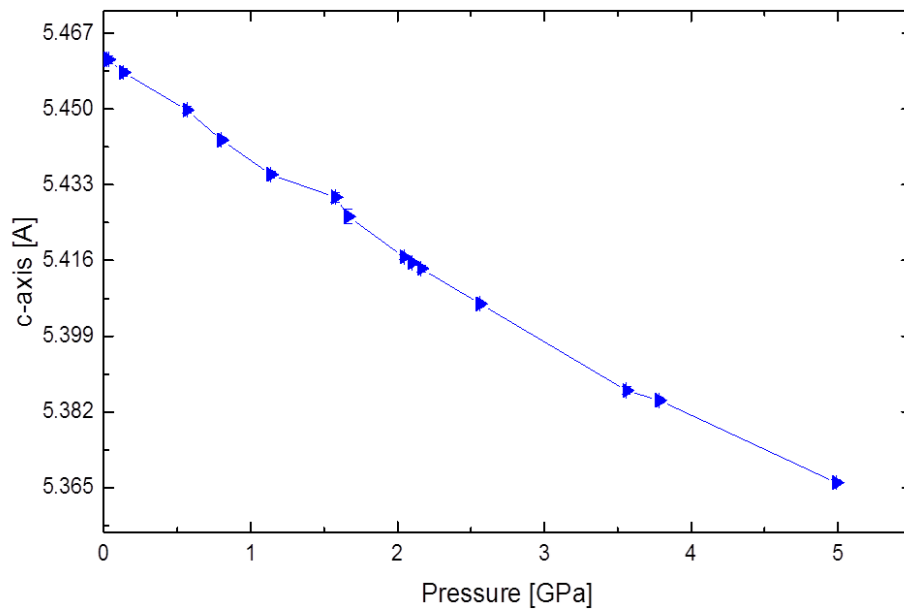
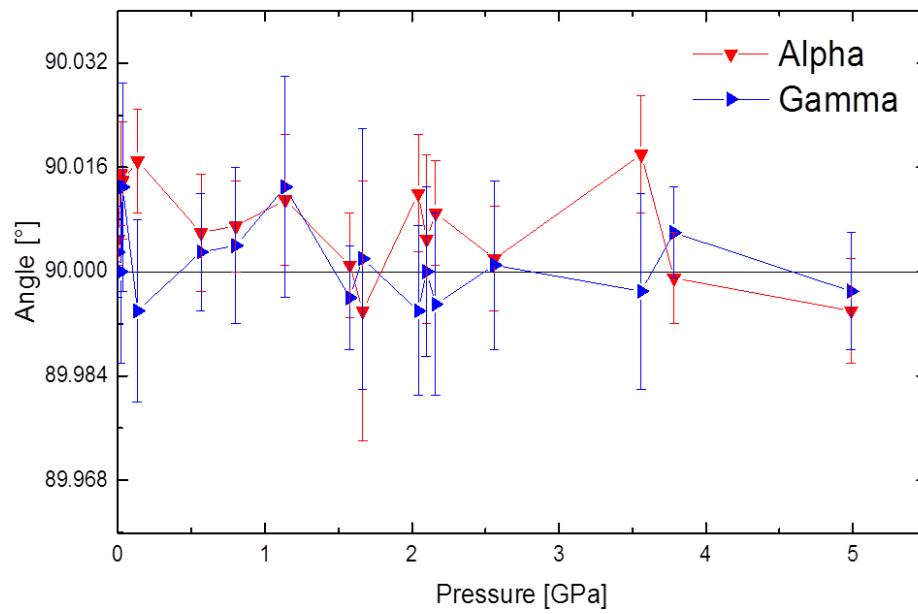
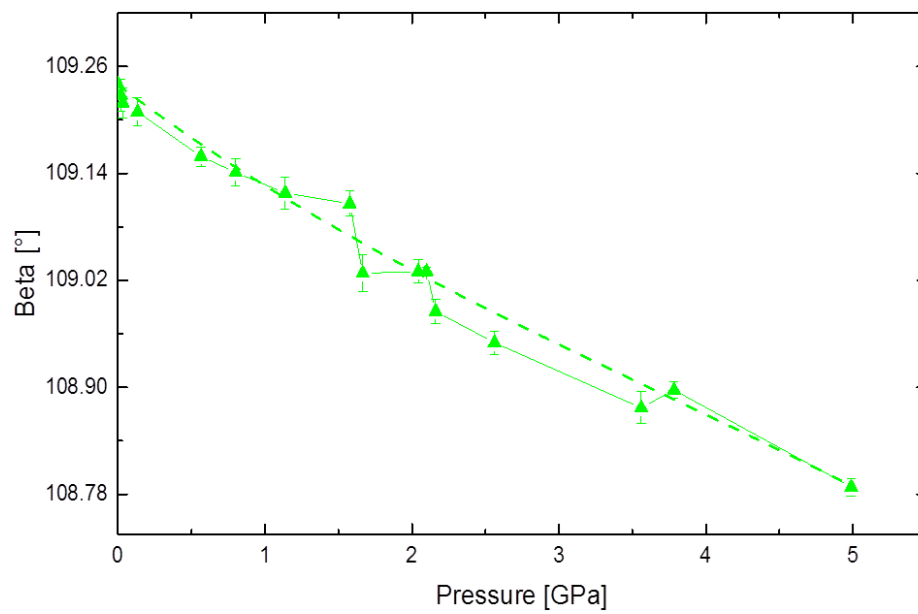


Figure 15: Compression of the c-axis.

Figure 16: Change of the α - and γ -angle during the compression.Figure 17: Change of the β -angle during the compression. The dashed line was inserted for guiding the eye.

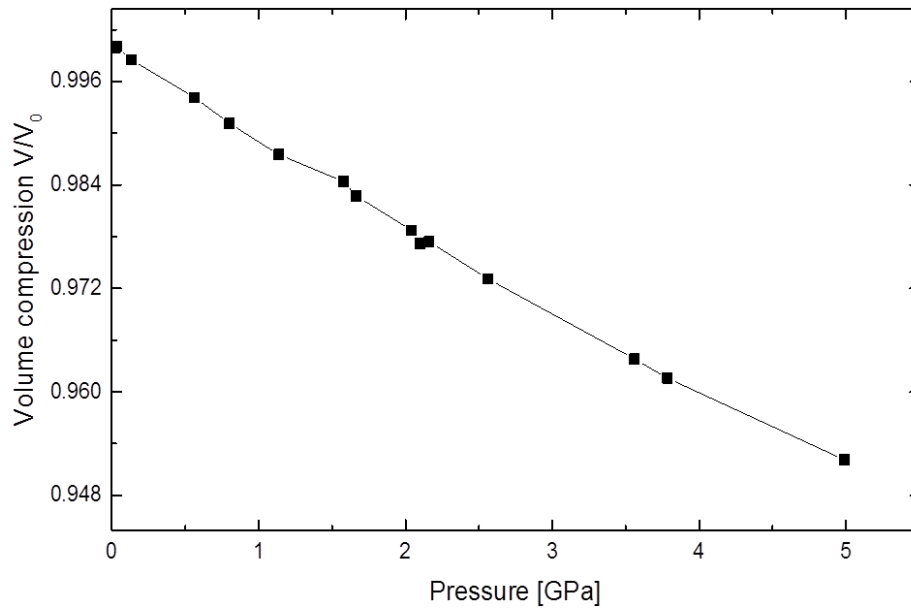


Figure 18: Relative compression of the unit-cell volume with respect to ambient conditions.

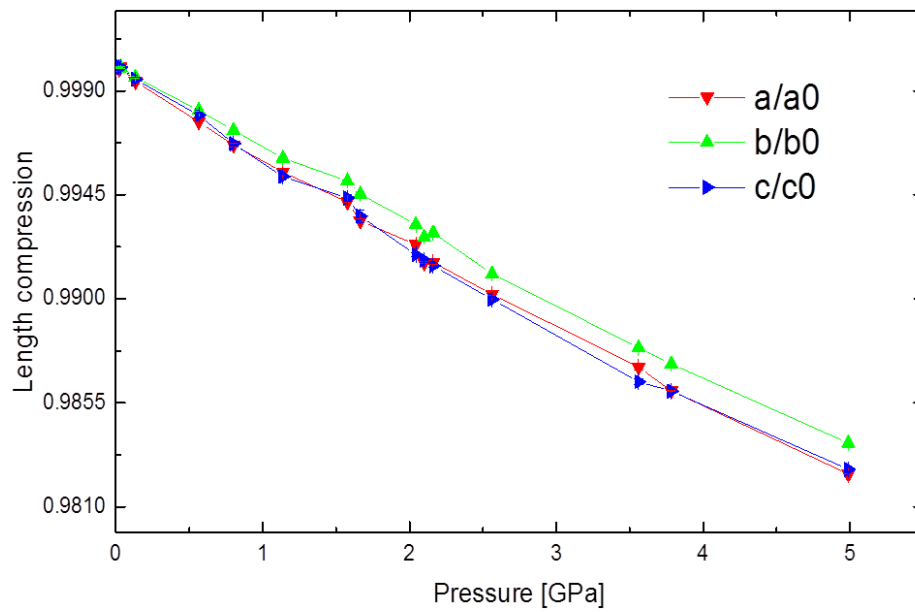


Figure 19: Relative compression of the crystallographic axes with respect to ambient conditions.

4 Discussion

4.1 Raman spectra

The obtained Raman spectra in Figure 1 do not show any conspicuous signs of a phase transition to occur within the experimental-covered pressure-range. The 0.0001 GPa spectra was obtained outside of the *ETH-DAC*. The additional peaks from the 0.0001 GPa to the 0.5 GPa spectra are methanol and ethanol bands which belong to the pressure fluid. As expected, Raman bands with a low shift do not significantly change their position with increased pressure, see Figure 2 and Table 12. The Raman bands with a higher shift change their position towards a higher Raman shift with pressure increase, also as expected. The data points were fitted with a linear function and show a continuous slope, which is a further indication that no phase transition occurs between 0.0001 GPa and 5.12 GPa.

[cm ⁻¹]	Symbol	Slope	[cm ⁻¹ /GPa]	Assignment	Sym.
71	■	0.53(12)	0.71(13)		
99	●	-0.15(12)	0.31(9)		
114	▲	-0.77(14)	0.74(15)	O-Si-O bending y	B_g^1
212	▼	1.06(8)	1.1(5)	O-Sc-O, O-Si-O bending x	A_g^3
372	◆	4.8(5)	5.4(9)	O-Sc-O bending	A_g^6
448	◀	5.37(12)	5.4(2)	O-Sc-O bending	B_g^8
554	▶	4.33(13)	4.46(4)	O-Sc-O, O-Si-O bending	B_g^{10}
903	●	5.34(13)	5.4(6)	Sc-O, Si-O stretching	A_g^{12}

Table 12: Changes of Raman shift with increasing pressure. Bands have been labeled according to Popović et al. (2005).

4.2 Compression behavior

The parameters of the third-order Birch-Murnaghan *EoS* are given in Table 13. The figures, which show the volume and axis compression are within their errors on a continuous line with no change in curvature. This indicates that no phase transition happened between 0.0001 GPa and 4.99 GPa, as already shown by the

Raman spectra. The unconstrained refinements of α and γ show that these two angles stick to 90° within their range of error, see Figure 3.3. These observations rule out a first or second order phase transition.

	V_0 [\AA^3]	K_0 [GPa]	K'
V	469.61(11)	83(2)	7.5(11)
	x_0 [\AA]	M_0 [GPa]	M'
<i>a</i>	10.001(14)	223(9)	27(5)
<i>b</i>	9.1046(7)	277(7)	9(4)
<i>c</i>	5.4613(3)	227(6)	24(4)

Table 13: EoS parameters of the third-order Birch-Murnaghan.

Three good structure-refinements at 0.0001, 4.94 and 9.51 GPa were done to gain additional insight into the crystal structure over a wider pressure range, see Table 4. The structure refinements reveal no indication of a change of space-group which further indicates the non-existence of a first order phase transition. Anisotropic refinement of germanium succeeded at all pressures scandium and oxygen only under ambient conditions. Lithium could not successfully anisotropic refined, most likely because of its few electrons. The increased anisotropic displacement parameters of germanium at higher pressures is most likely due to partial insufficient data resolution because of restrictions set by the design of the *ETH-DAC*.

A method for verifying the order of any isothermal equation-of-state is the f-F plot of the Eulerian strain (Angel et al., 2000). The inclination of the linear regression lines confirms the use of a third order equation of state, see Figure 20. Note the reduction of uncertainty of the norm pressure F_E . This is because the increase of the Eulerian strain f is linked to increase of pressure and the uncertainty of F_E is inverse proportional to pressure.

A prominent feature of the $P2_1/c$ crystal structure of *LSG* are the two distinctive Ge-tetrahedron chains. The tetrahedrons of the chains are corner-connected to

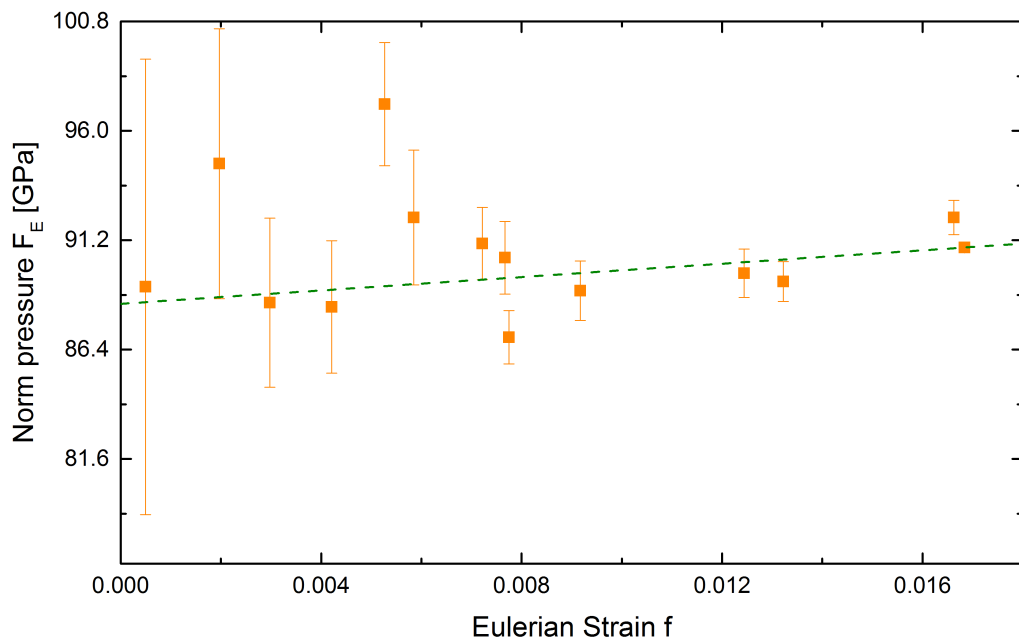


Figure 20: Eulerian strain of the measured pressure points after Angel et al. (2000).

their surrounding polyhedrons. Both chains run parallel to the c -axis. All chains combined form a (100) layer through the unit cell. According to the nomenclature of Cameron and Papike (1981), the A-chain is s -rotated and the B-chain is o -rotated. Under pressure, the bridging oxygen ions from the A-chain move along the a -axis towards the center of their respective unit cell and closer to metal ions, see Figures 3 and 4. The visible change of the chain-interconnection is hardly noticeable when viewed along the a -axis, see Table 9 and Figures 7 and 8. The bridging oxygen ions in the B-chain move in a layer parallel to the b - and c -axis with increased pressure. As visible in Figures 9 and 10, using the same projection as before, a visual change in the chain-interconnection is noticeable. The bridging and OB1 oxygen ions contribute most to this change. The B-chain shows a larger change of angular changes than the A-chain, see Figure 21. The OA3-OA3-OA3 angle is stiffer with respect to the GeA-OA3-GeA angle while in the B-chain the OB3-OB3-OB3 angle is softer with respect to the GeB-OB3-GeB angle.

The M1 and M2 position are both in a 6-fold coordination. Lithium at the M1 position is located in a higher angular distorted octahedron with respect to the

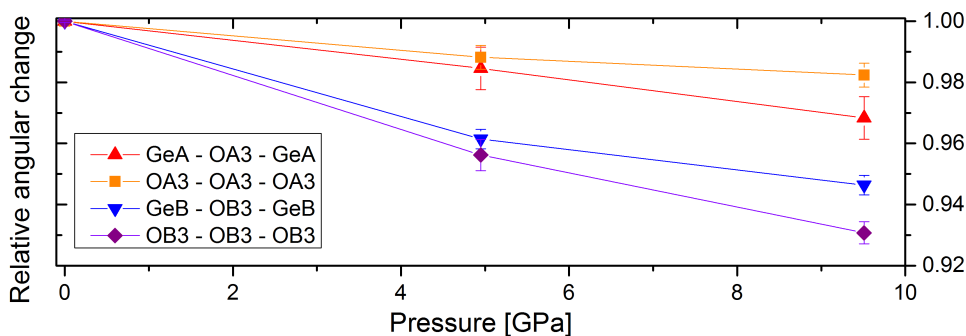


Figure 21: Relative angular changes of selected chain angles.

scandium octahedron at the M2 position. The Li-octahedrons are isolated from each other and are edge-connected to three Sc-octahedrons. The Sc-octahedrons are edge-connected to two Sc-octahedrons and three Li-octahedrons. The edge-connected Sc-octahedrons form a chain which runs parallel to the tetrahedron-chains. By comparing the calculated distortion parameters in Table 10 with the currently only work, which mentions distortion parameters of clinopyroxenes, of Ullrich et al. (2009b), similar distortions can be observed, save the Li-octahedron.

Anderson and Nafe (1965) showed a method of predicting the bulk modulus of oxide compounds by the relationship of volume and bulk modulus. By applying this method on the currently latest publications of bulk modulus data from clinopyroxene structures and sorting this data according to chemistry, the resulting plot (figure 22) reveals a linear trend for the clinopyroxene groups with great deviations. Though not accurate, this method is useful for an approximate estimation.

Nestola et al. (2012) showed a possibility to estimate the bulk modulus of clinopyroxene structures with a higher precision. Nestola et al. (2012) plotted the volume at ambient conditions versus the calculated relative compressibility at 10 GPa of until then investigated two-metal clinopyroxenes. A distinctive linear trend for calcium and sodium pyroxenes was the result. The data points show a lesser deviation from the trend line compared to Anderson and Nafe (1965). This plot implicates that the relative compression is primary influenced by the M2 position while the offset is dominated by the M1 position. Figure 23 advances this idea and adds all since then published compression data of clinopyroxene structures

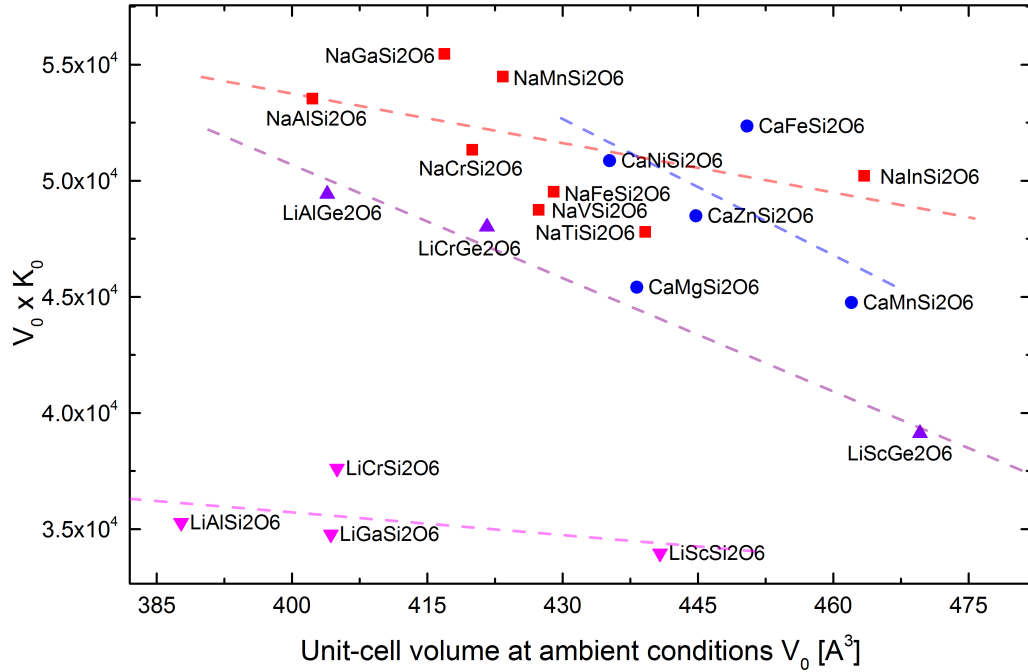


Figure 22: Predictions of the bulk modulus for all current high-pressure studies of two-metal clinopyroxenes. Sources: LiScSi₂O₆ and LiAlSi₂O₆ by Arlt and Angel (2000), LiAlGe₂O₆ and LiCr₂O₆ by Artac et al. (2014), NaGaSi₂O₆ by McCarthy (2007), CaNiSi₂O₆ and NaFeSi₂O₆ by Nestola et al. (2005), NaAlSi₂O₆ by Nestola et al. (2006), LiGaSi₂O₆ by Nestola et al. (2008), CaMnSi₂O₆ and CaZnSi₂O₆ by Nestola et al. (2010), NaMnSi₂O₆ by Nestola et al. (2012), NaInSi₂O₆ by Periotto et al. (2012), LiCrSi₂O₆ by Periotto et al. (2013), NaCrSi₂O₆ by Posner et al. (2014), NaVSi₂O₆ by Ullrich et al. (2009a), NaTiSi₂O₆ by Ullrich et al. (2010), CaFeSi₂O₆ and CaMgSi₂O₆ by Zhang et al. (1997), LiScGe₂O₆ from this study.

with two distinctive metal ions. All values are calculated from the given equation of state parameters. If a phase transition occurred below 10 GPa, the high-pressure phase parameters were used. NaTiSi₂O₆ was omitted from calculating the trend lines because its compression behavior is strongly influenced by the interaction of the d-electrons of Ti³⁺ (Ullrich et al., 2010) and therefore not fit for comparison with clinopyroxenes which do not show this effect. CaMgSi₂O₆ was also omitted from calculations because of its suspicious high offset compared to other Ca-pyroxenes. This offset could be a simple variation within the Ca-pyroxenes. Another explanation could be that Ca-pyroxenes with transition metals have a different compression behavior than those with alkaline earth metals. However, the speculations of trend deviations are not a subject of this work, further research is required.

With the more complete data set, the first noticeable difference is the smaller devi-

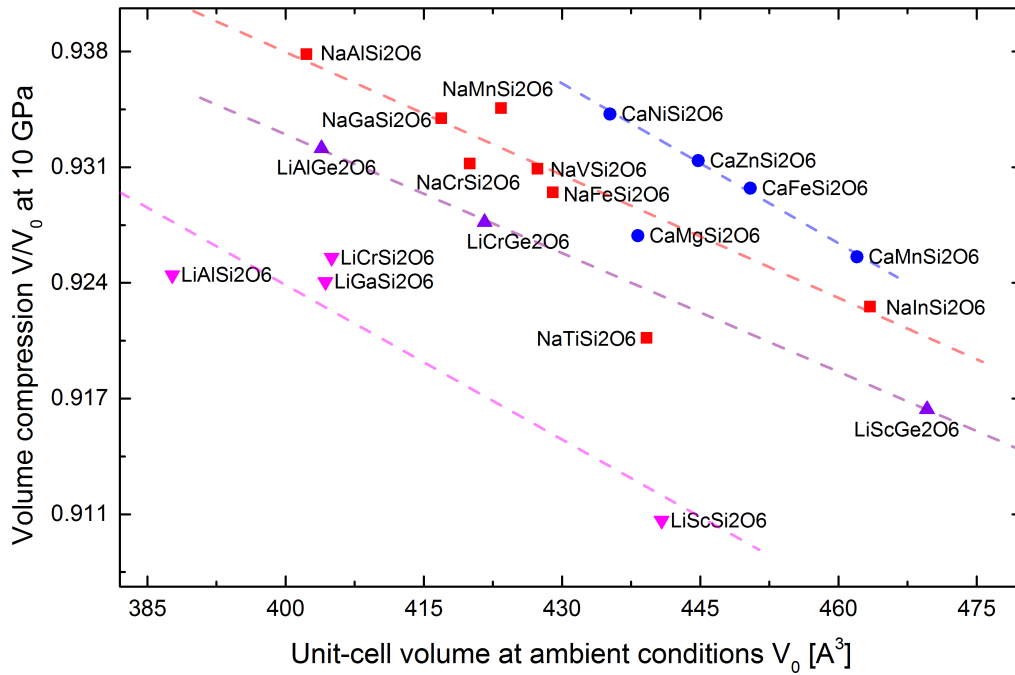


Figure 23: Predictions of the bulk modulus for all current high-pressure studies of two-metal clinopyroxenes. Sources are the same as in figure 22.

ation of the data points from the trend lines, $\text{CaFeSi}_2\text{O}_6$ or NaVSi_2O_6 for instance. This figure continues the trend, that the M1-position defines the offset the linear trend. These trend lines are almost parallel to each other. Furthermore it shows that the offset is also depended on the ion in the tetrahedron chain. The results of this compression study about $\text{LiScGe}_2\text{O}_6$ are well in line with the prediction made based on Artac et al. (2014).

5 Appendix

References

- Anderson, O. L. and Nafe, J. E. (1965). The bulk modulus-volume relationship for oxide compounds and related geophysical problems. *Journal of Geophysical Research*, 70(16):3951–3963.
- Angel, R., Allan, D., Miletich, R., and Finger, L. (1997). The use of quartz as an internal pressure standard in high-pressure crystallography. *Journal of Applied Crystallography*, 30(4):461–466.
- Angel, R., Downs, R., and Finger, L. (2000). High-temperature–high-pressure diffractometry. *Reviews in mineralogy and geochemistry*, 41(1):559–597.
- Angel, R. and Finger, L. (2010). Single: a program to control single-crystal diffractometers. *Journal of Applied Crystallography*, 44(1):247–251.
- Angel, R. J., Bujak, M., Zhao, J., Gatta, G. D., and Jacobsen, S. D. (2007). Effective hydrostatic limits of pressure media for high-pressure crystallographic studies. *Journal of Applied Crystallography*, 40(1):26–32.
- Arlt, T. and Angel, R. (2000). Displacive phase transitions in c-centred clinopyroxenes: spodumene, $\text{LiScSi}_2\text{O}_6$ and ZnSiO_3 . *Physics and Chemistry of Minerals*, 27(10):719–731.
- Artac, A., Miletich-Pawliczek, R., Nestola, F., Redhammer, G. J., and Secco, L. (2014). Elastic behaviour and high-pressure phase transition of the $P2_1/n$ $\text{LiAlGe}_2\text{O}_6$ pyroxene.
- Boehler, R. and De Hantsetters, K. (2004). New anvil designs in diamond-cells. *High Pressure Research*, 24(3):391–396.
- Cameron, M. and Papike, J. (1981). Structural and chemical variations in pyroxenes. *American Mineralogist*, 66(1-2):1–50.

- Hamilton, W. C. (1974). Angle settings for four-circle diffractometers. *International Tables for x-ray Crystallography*, 4:273–284.
- Mao, H., Xu, J.-A., and Bell, P. (1986). Calibration of the ruby pressure gauge to 800 kbar under quasi-hydrostatic conditions. *Journal of Geophysical Research: Solid Earth (1978–2012)*, 91(B5):4673–4676.
- McCarthy, A. C. (2007). *Behavior of sodium clinopyroxenes under compression*. ProQuest.
- Miletich, R., Allan, D. R., and Kuhs, W. F. (2000). High-pressure single-crystal techniques. *Reviews in mineralogy and geochemistry*, 41(1):445–519.
- Nestola, F., Ballaran, T. B., Angel, R. J., Zhao, J., and Ohashi, H. (2010). High-pressure behavior of Ca/Na clinopyroxenes: The effect of divalent and trivalent 3d-transition elements. *American Mineralogist*, 95(5-6):832–838.
- Nestola, F., Ballaran, T. B., Liebske, C., Bruno, M., and Tribaudino, M. (2006). High-pressure behaviour along the jadeite $\text{NaAlSi}_2\text{O}_6$ –aegirine $\text{NaFeSi}_2\text{O}_6$ solid solution up to 10 gpa. *Physics and Chemistry of Minerals*, 33(6):417–425.
- Nestola, F., Ballaran, T. B., and Ohashi, H. (2008). The high-pressure $C2/c - P2_1/c$ phase transition along the $\text{LiAlSi}_2\text{O}_6 - \text{LiGaSi}_2\text{O}_6$ solid solution. *Physics and Chemistry of Minerals*, 35(8):477–484.
- Nestola, F., Ballaran, T. B., Tribaudino, M., and Ohashi, H. (2005). Compressional behaviour of $\text{CaNiSi}_2\text{O}_6$ clinopyroxene: bulk modulus systematic and cation type in clinopyroxenes. *Physics and Chemistry of Minerals*, 32(3):222–227.
- Nestola, F., Nardini, L., Pasqual, D., Periotto, B., Lucchetti, G., Miletich, R., and Belmonte, D. (2012). Compressibility of $\text{NaMnSi}_2\text{O}_6$: The role of electronic isovalency for the validity of bulk-modulus–volume relationship. *Solid State Sciences*, 14(8):1036–1039.

- Periotto, B., Angel, R. J., Nestola, F., Balić-Žunić, T., Fontana, C., Pasqual, D., Alvaro, M., and Redhammer, G. J. (2013). High-pressure x-ray study of $\text{LiCrSi}_2\text{O}_6$ clinopyroxene and the general compressibility trends for clinopyroxenes. *Physics and Chemistry of Minerals*, 40(5):387–399.
- Periotto, B., Nestola, F., Balić-Žunić, T., Pasqual, D., Alvaro, M., and Ohashi, H. (2012). High-pressure behavior of $\text{NaInSi}_2\text{O}_6$ and the influence of me^{3+} on the compressibility of $\text{NaMe}^{3+}\text{Si}_2\text{O}_6$ silicates. *Solid State Communications*, 152(2):132–137.
- Popović, Z., Konstantinović, M., Popov, V., Cantarero, A., Dohčević-Mitrović, Z., Isobe, M., and Ueda, Y. (2005). Optical phonons in the $\text{NaTiSi}_2\text{O}_6$ oxide with $s = \frac{1}{2}$ spin chains. *Physical Review B*, 71(22):224302.
- Posner, E. S., Dera, P., Downs, R. T., Lazarz, J. D., and Irmen, P. (2014). High-pressure single-crystal x-ray diffraction study of jadeite and kosmochlor. *Physics and Chemistry of Minerals*, pages 1–13.
- Renner, B. and Lehmann, G. (1986). Correlation of angular and bond length distortions in TO_4 units in crystals. *Zeitschrift für Kristallographie*, 175(1-2):43–59.
- Sheldrick, G. M. (1997). Shelx-97, program for crystal structure solution and refinement. *University of Göttingen, Germany*, page 1456.
- Ullrich, A., Miletich, R., Balić-Zunic, T., Olsen, L., Nestola, F., Wildner, M., and Ohashi, H. (2010). $(\text{Na}, \text{Ca})(\text{Ti}^{3+}, \text{Mg})\text{Si}_2\text{O}_6$ -clinopyroxenes at high pressure: influence of cation substitution on elastic behavior and phase transition. *Physics and Chemistry of Minerals*, 37(1):25–43.
- Ullrich, A., Miletich, R., Nestola, F., Weikusat, C., and Ohashi, H. (2009a). Lattice compression and structural behavior of NaVSi_2O_6 clinopyroxene to 11 GPa. *American Mineralogist*, 94(4):557–564.
- Ullrich, A., Schranz, W., and Miletich, R. (2009b). The nonlinear anomalous lattice elasticity associated with the high-pressure phase transition in spodumene:

a high-precision static compression study. *Physics and Chemistry of Minerals*, 36(10):545–555.

Zhang, L., Ahsbahs, H., Hafner, S. S., and Kutoglu, A. (1997). Single-crystal compression and crystal structure of clinopyroxene up to 10 GPa. *American Mineralogist*, 82(3):245–258.

List of Figures

1	Raman spectra at different pressures	11
2	Shift of selected Raman-bands	12
3	Crystal structure along [001] at 0 GPa	19
4	Crystal structure along [001] at 9.51 GPa	20
5	Crystal structure along [010] at 0 GPa	21
6	Crystal structure along [010] at 9.51 GPa	22
7	Germanate tetrahedral A-chain along [100] at 0 GPa	22
8	Germanate tetrahedral A-chain along [100] at 9.51 GPa	23
9	Germanate tetrahedral B-chain along [100] at 0 GPa	23
10	Germanate tetrahedral B-chain along [100] at 9.51 GPa	23
11	Octahedral layer [100] at 0 GPa	24
12	Compression of the unit-cell volume	26
13	Compression of the a-axis	26
14	Compression of the b-axis	27
15	Compression of the c-axis	27
16	Change of the α - and γ -angle during the compression	28
17	Change of the β -angle during the compression	28
18	Relative compression of the unit-cell volume	29
19	Relative compression of the crystallographic axes	29
20	Eulerian Strain	32
21	Relative angular changes of selected chain angles	33
22	Comparison of clinopyroxenes after Anderson and Nafe (1965)	34
23	Comparison of clinopyroxenes after Nestola et al. (2012)	35

List of Tables

1	Comparison of diamond-anvils	4
2	<i>ETH-DAC</i> loadings summary	6
3	Experimental setup for Raman-spectrometers	7
4	Experimental details of the crystal lattices, intensity data collec- tions and structure refinements	10
5	Atomic coordinates at different pressures	14
6	Anisotropic displacement parameters of germanium	15
7	Anisotropic displacement parameters of scandium and oxygen	15
8	Selected inter-atomic distances	16
9	Selected bond angles	18
10	Polyhedral distortion parameters	18
11	Tabular result of lattice compression	25
12	Raman shift changes with pressure	30
13	Equation-of-state parameters	31

Deutsche Zusammenfassung

Der synthetische Klinopyroxen $\text{LiScGe}_2\text{O}_6$ wurde mittels in-situ Hochdruck Raman Spektroskopie und Röntgenbeugungsmethoden untersucht. Drei Strukturverfeinerungen bei 0.0001, 4.94 und 9.51 GPa wurden durchgeführt. Sie bestätigen die Raumgruppe $P2_1/c$; Die Gitterkonstanten sind bei 0.0001 GPa $a = 9.9999(8)$ Å, $b = 9.1040(2)$ Å, $c = 5.4610(2)$ Å, $\beta = 109.240(2)^\circ$. Reihen von Röntgenbeugungsmessungen der Gitterkonstanten und Raman-Spektren wurden über den Druckbereich von 0.0001 bis 4.99(1) GPa aufgenommen. Diese Daten der Röntgenuntersuchung zeigen einen kontinuierlichen Verlauf und deuten damit eine Abwesenheit einer Phasentransformation an. Diese Beobachtung deckt sich mit den Ergebnissen der Strukturverfeinerungen. Die Gitterkonstanten wurden mit der Birch-Murnaghan Zustandsgleichung dritter Ordnung verfeinert und ergab $V_0 = 469.61(11)$ Å³, $K_0 = 83(2)$ GPa und $K' = 7.5(11)$. Die Ramanspektren unterstützen die Beobachtungen der Röntgendaten. Die Ergebnisse wurden mit aktuellen Hochdruckstudien von Klinopyroxenen verglichen und zeigen eine Fortsetzung der aufgestellten Trends des Hochdruckverhaltens von Klinopyroxenen.

Curriculum vitae

Personal data

Name: Gregor Hofer
Address: Webgasse 1/8 1060 Vienna, Austria
Date of birth: 14.01.1988, Vienna, Austria
Mobile: +4369912542703
Email: gregorhofer@gmx.at
Nationality: Austria
Marital status: Single

Education

Since 10/2012 Master studies in mineralogy and crystallography at the University of Vienna

2009 – 2012 Bachelor studies in earth sciences at the University of Vienna

2002 – 2007 Technical high school Spengergasse for IT, specialized in network technology

1998 – 2002 Grammar school Amerlingstraße

1994 – 1998 Elementary school St. Marien

Employment history:

06/2013 – date Student trainee at the X-Ray Center of the **Technical University of Vienna**

- Residual stress analysis with x-rays
- Qualitative phase analysis

10/2013 – 01/2014 Tutor for „Mineralogy and crystallography for teaching biology“ at the **University of Vienna**

- Supporting students during exercises

09/2013 Laboratory and pilot plant assistant at **Richard Klinger Dichtungstechnik GmbH & Co. KG**

- Quantitative sulphate and chloride analysis of all used resources and produced materials
- Creating resource and material reference samples under the microscope
- Supporting work in laboratory and pilot plant

03/2013 – 06/2013 Tutor for „Mineralogy and crystallography for teaching biology“

- at the **University of Vienna**

 - Supporting students during exercises
- 03/2013 – 06/2013** Tutor for „Experiments in earth sciences for teaching biology“ at the **University of Vienna**

 - Supporting students during exercises
- 03/2012 – 03/2013** Freelancer at **Global2000** as environmental communicator

 - Mentoring workshops and presenting current issues of the environment
- 02/2013** Laboratory and pilot plant assistant at **Richard Klinger Dichtungstechnik GmbH & Co. KG**

 - Creation and testing of a new database regrading environmental clearances of resources and materials
 - Creating resource and material reference samples under the microscope
 - Supporting work in laboratory and pilot plant
- 09/2012** Laboratory and pilot plant assistant at **Richard Klinger Dichtungstechnik GmbH & Co. KG**

 - Creating sample pieces with the means of a hydraulic press and calender
 - Evaluation of sample pieces which were exposed to different physical and chemical conditions
 - Creating resource and material reference samples under the microscope
 - Supporting work in laboratory and pilot plant
- 10/2012 – 01/2013** Tutor for „Mineralogy and crystallography for teaching biology“ at the **University of Vienna**

 - Supporting students during exercises
- 10/2012 – 01/2013** Tutor for „Experiments in earth sciences for teaching biology“ at the **University of Vienna**

 - Supporting students during exercises
- 03/2012 – 05/2012** Freelancer at the paleontology department at the **University of Vienna**

 - 3D measurements of microfossils
- 03/2012 – 06/2012** Tutor for „Mineralogy and crystallography for teaching biology“ at the **University of Vienna**

 - Supporting students during exercises
- 10/2011 – 01/2012** Tutor for „Mineralogy and crystallography for teaching biology“ at the **University of Vienna**

 - Supporting students during exercises

- 10/2011 – 01/2012** Tutor for „Experiments in earth sciences for teaching biology“ at the **University of Vienna**
- Supporting students during exercises
- 09/2011** Laboratory and pilot plant assistant at **Richard Klinger Dichtungstechnik GmbH & Co. KG**
- Creating resource and material reference samples under the microscope
 - Creating sample pieces with the means of a hydraulic press and calender
 - Evaluation of sample pieces which were exposed to different physical and chemical conditions
 - Supporting work in laboratory and pilot plant
- 08/2011** Cooperation with **UNHCR** during the 22nd World Scout Jamboree
- Creating situation awareness regarding refugees for teenagers
- 10/2010 – 01/2011** Tutor for „Crystallography and mineralogy“ at the **University of Vienna**
- Supporting students during exercises
- 10/2010 – 12/2010** Freelancer at **Alexander Kovar Sachverständigung**
- PC hardware repair
- 07/2010 – 09/2010** Intern at the **Austrian Post Office**
- Delivering mail
- 2009** Different kinds of one-day-jobs
- Catering
 - Supporting staff during conferences
- 06/2009 – 07/2009** Freelancer at **AComp**
- All kinds of programming work
- 04/2009 – 05/2009** Insurance agent at **VFG**
- Advising potential customers
- 01/2009 – 03/2009** Freelancer at **Alexander Kovar Sachverständigung**
- PC hardware repair
- 08/2008 – 11/2008** Freelancer at **AComp**
- All kinds of programming work
- 10/2007 – 06/2008** Regular civil service **SPZ Schwarzinger gasse** (a school for special needs)
- Care for children

- 08/2006** Intern at **OMV Exploration & Production**
- Creating environmental reports
- 07/2005** Intern at **OMV Solutions**
- Network administration
- 07/2004** Intern at **OMV Solutions**
- Database administration

Scientific Skills

- **Single crystal diffraction methods:** High-pressure studies and high-pressure structure refinement with point and area detectors
- **Powder diffraction methods:** Residual stress analysis, phase identification
- **Raman spectroscopy:** Advanced user, phase identification
- **Scanning electron microscopy:** Advanced user
- **IR spectroscopy:** Basic user

Master thesis Compressibility and high-pressure behavior of spodumene-type
12/2014 – 07/2014 $\text{LiScGe}_2\text{O}_6$
 Supervisor: Prof. Dr. R. Miletich-Pawliczek

Areas of interest

-) Materials under unusual conditions
-) Impact of particle radiation on crystal structures
-) “Unusual” crystal structures like frustrated structure, kagome-lattices, cage structures (like clathrates and zeolites)
-) Impact of mechanical strain and wear on materials

Publications

T. Pippinger, R. Miletich, H. Effenberger, G. Hofer, P. Lotti M. Merlini: High-pressure polymorphism and structural transitions of norsethite, $\text{BaMg}(\text{CO}_3)_2$, about to be published, DOI: 10.1007/s00269-014-0687-8

Presentations, attended conferences and workshops

- 05/2014** Public presentation of my master thesis at the University of Vienna
- 07/2013** “Corals-2013: Conference and workshop on Raman and Luminescence Spectroscopy” at the University of Vienna
- 02/2013** “29th Annual Technical Sessions and 29th Annual General Meeting of the Geological Society of Sri Lanka” in Kandy, Sri Lanka

05/2012 "European Geosciences Union 2012 General Assembly" in Vienna

Miscellaneous

IT software skills	Windows, LINUX/UNIX, Microsoft Office, LibreOffice, artistic 3D modeling, GIMP, different kinds of subject-specific software (HighScorePlus, ATOMS, SHELX, FINDIT, EoSFit, PeakFit)
IT programming skills	C#, bash, Java, LaTeX, C, php/html, Delphi (basics), C++ (basics), python (basics)
Languages	German, native speaker Englisch, fluent French, basics
Driving licences	A (Motorcycle) and B (car)
Personal interests	Scouting, flying, hiking, running